ENERGY MANAGEMENT IN ENERGY HARVESTING WIRELESS SENSOR NODES WITH LIFETIME CONSTRAINTS

A THESIS SUBMITTED TO

THE GRADUATE SCHOOL OF ENGINEERING AND SCIENCE

OF BILKENT UNIVERSITY

IN PARTIAL FULFILLMENT OF THE REQUIREMENTS FOR

THE DEGREE OF

MASTER OF SCIENCE

IN

ELECTRICAL AND ELECTRONICS ENGINEERING

By

Çağlar Tunç

June, 2016

ENERGY MANAGEMENT IN ENERGY HARVESTING WIRELESS SENSOR NODES WITH LIFETIME CONSTRAINTS
By Çağlar Tunç
June, 2016

We certify that we have read this thesis and that in our opinion it is fully adequate, in scope and in quality, as a thesis for the degree of Master of Science.

Nail Akar(Advisor)

Ezhan Karaşan

Murat Alanyalı

Approved for the Graduate School of Engineering and Science:

Levent Onural
Director of the Graduate School

ABSTRACT

ENERGY MANAGEMENT IN ENERGY HARVESTING WIRELESS SENSOR NODES WITH LIFETIME CONSTRAINTS

Çağlar Tunç
M.S. in Electrical and Electronics Engineering
Advisor: Nail Akar
June, 2016

Advancements in the "Internet of Things (IoT)" concept enables large numbers of low-power wireless sensors and electronic devices to be connected to the Internet and outside world over a wide area wireless network without a need for human interaction. Using rechargeable batteries with energy harvesting to power these wireless sensors has been shown to preserve the self-sustainability and self-sufficiency of a sensor node and prolong its lifetime, hence the whole network it belongs to. However, it brings the question of how to intelligently manage the energy in the battery so that the node maintains its functionalities by keeping the battery level over zero for an extended duration of time, known as the life-horizon. We propose a risk-theoretic Markov fluid queue model to compute the battery outage probability of a wireless sensor node for a given finite life-horizon. The proposed method enables the performance evaluation of a wide spectrum of energy management policies including those with adaptive sensing rate (or duty cycling). In this model, the node gathers data from the environment according to a Poisson process whose rate is to depend on the instantaneous battery level and/or the state of the energy harvesting process (EHP) which is characterized by a Continuous time Markov Chain (CTMC). Moreover, an engineering methodology is proposed by which optimal threshold-based adaptive sensing rate policies are obtained that maximize the information sensing rate of the sensor node while meeting lifetime constraints given in terms of battery outage probabilities. Numerical results are presented for the validation of the analytical model and also the proposed engineering methodology, using two-state CTMC-based EHPs.

Keywords: wireless sensor nodes, Internet of Things, energy harvesting, Markov fluid queues, risk theory, battery outage probability, adaptive duty cycling.

ÖZET

ENERJİ HARMANLAYAN KABLOSUZ ALGILAMA DÜĞÜMLERİNDE YAŞAM SÜRESİ KISITLAMALI ENERJİ YÖNETİMİ

Çağlar Tunç
Elektrik ve Elektronik Mühendisliği, Yüksek Lisans
Tez Danışmanı: Nail Akar
Haziran, 2016

"Nesnelerin İnterneti (IoT)" kavramındaki gelişmeler, düşük güçte çalışan çok sayıda kablosuz algılayıcının ve elektronik cihazın insan etkileşimine ihtiyaç duymadan İnternet ve dış dünyaya bağlanmasını sağlar. Kablosuz algılayıcılarda enerji harmanlayan pillerin kullanımının algılayıcı düğümünün, dolayısıyla ait olduğu ağın ömrünün uzamasını ve kendi kendini devam ettirebilmesini sağladığı gösterilmiştir. Bununla birlikte ortaya düğümün yaşam ufku olarak bilinen geniş bir zaman dilimi boyunca pilini tüketmeden işlevsel kalması sağlanacak şekilde pildeki enerji miktarının nasıl akıllıca idare edileceği sorusu çıkmaktadır. Bu tezde, kablosuz algılama düğümlerinde sonlu bir yaşam ufkunda pil tükenmesi olasılığını hesaplayan risk teorisi tabanlı bir Markov akışkan kuyruk modeli önerdik. Önerilen yöntem, uyarlanır algılama sıklığı (ya da iş çevrimi) da dahil olmak üzere çeşitli enerji yönetim mekanizmalarının performans değerlendirmesini mümkün kılmaktadır. Bu modelde düğüm bulunduğu ortamdan, sıklığı anlık pil miktarına ve/veya Sürekli Zamanlı Markov Zinciri (CTMC) ile modellenen enerji harmanlama sürecinin (EHP) durumuna bağlı olan bir Poisson sürecine göre veri toplar. Öte yandan, pil tükenmesi olasılığı cinsinden verilen yaşam süresi gerekliliklerini karşılarken bilgi algılama sıklığını eniyilemeyi hedefleyen, eşik-tabanlı uyarlanır algılama sıklığı politikalarını veren bir mühendislik yöntemi de geliştirdik. İki fazlı CTMC tabanlı EHP kullanarak, sayısal modeli ve önerilen mühendislik yöntemini doğrulayan sayısal sonuçlar sunduk.

Anahtar sözcükler: kablosuz algılama düğümleri, Nesnelerin İnterneti, enerji harmanlama, Markov akışkan kuyrukları, risk teorisi, pil tükenme olasılığı, uyarlanır iş çevrimi.

Acknowledgement

First and foremost, I would like to express my gratitude to my supervisor Prof. Nail Akar for his comprehensive guidance in the development of this thesis and more importantly for his encouragement and motivation along my graduate life.

I would also like to thank my thesis committee: Prof. Ezhan Karaşan and Prof. Murat Alanyalı, for reading this thesis and sharing their insightful comments and suggestions.

I would like to acknowledge TÜBİTAK for funding this thesis with BİDEB 2228 and ARDEB 1001 (under the project number 115E360) programs.

None of this would have been possible without the support of my family. I am grateful to them for constantly keeping me motivated and determined throughout this endeavor.

I would like to thank my oldest and dearest friends Özge Yalçınkaya, Gizem Orta and Arman Tekinalp for being there for me whenever I needed them throughout my entire life.

I would like to thank Esra Aşcıgil for her motivational support in my stressful times.

Last but not least, I would like to thank my fiancée Öykü Arkan and her family for all the joy and meaning they have added to my life.

To the loving memories of my grandfathers,
Mehmet Zeki Demirel and İbrahim Tunç

Contents

List of Figures

List of Tables

Chapter 1

Introduction

The phrase "Internet of Things (IoT)" was first coined by British technology pioneer Kevin Ashton in 1999 during a presentation about supply chain management at Procter & Gamble (P&G) [1]. As Ashton states in his article [1], albeit the term has transformed into various meanings and undertaken different roles in different contexts, its key feature has remained unchanged: computers gathering and processing their own information without a need for human intervention.

IoT is currently one of the most appealing and emerging concepts in the engineering literature that is related to all kinds of technologies which aim to enable everyday objects around us to be permanently connected to each other on a large scale network and to the outside world over the Internet, typically without a need for human interaction [2–4]. In general, the devices in IoT systems, which consist of sensors, wireless transceivers, power supplies (typically battery and/or capacitor) and information processing units, are connected in an IoT network structure with unique identifiers in IP domain. Considering the increasing number of the devices in IoT world, which is estimated to grow up to 25 billion in a few years [5], and the phasing in of IPv6 architecture which will permit even a larger number of connected "things", IoT will clearly be one of the most prominent concepts of the next decades.

Complying with the Ashton's emphasis in [1] on the importance of the computers that can see, hear and smell the world for themselves, one of the most widespread application areas of today's IoT systems is to monitor the sensory information of an environment with the help of the embedded sensors and track this information remotely over the Internet by using IoT facilities [2,4,6]. In fact, the application areas and key concepts of sensors and IoT systems overlap to a great extent such that sensor networks are generally considered as a subset of IoT systems in telecommunication context as in [4]. Although sensor networks have been comprehensively studied in the literature since late 1970s, advancement in IoT technologies gives rise to new research directions in sensor networks and their applications [7].

1.1 Wireless Sensor Networks

Wireless Sensor Networks (WSNs) refer to an interconnection of a large number of Sensor Nodes (SNs) each of which is deployed for the purpose of gathering sensory information regarding the located environment and disseminating this information across the WSN [8, 9]. WSNs target a wide spectrum of applications including indoor/outdoor environment monitoring, target tracking, logistics support, robotics, etc. [10]. As WSNs, which comprise sensor nodes communicating with a common sink node in a peer-to-peer manner or according to a certain topology, blend with IoT technologies, environmental monitoring and information transfering over WSNs via the Internet becomes much more easier due to the remote accessibility and self-sustainability of the structure [11].

One of the main concerns in the telecommunications literature regarding WSNs is to control the energy consumption of the SNs to prolong the lifetime of the individual SNs and thus that of the WSN they belong to [12,13]. Energy management in traditional non self-rechargeable battery powered wireless sensor networks have attracted vast attention in the literature for a few decades; where sensor nodes in a network have to keep their batteries "alive" by avoiding operating too aggresively which may on the other hand compromise the network performance in terms of the overall amount of data gathered [14–16]. Despite there exists studies on how to prolong the battery, hence network lifetimes of battery-powered sensor nodes, the need for human interaction in traditional batteries for replacing or recharging purposes significantly restricts their application areas.

In order to deal with this issue and improve the performance of SNs, a promising technology is to use renewable energy sources such as solar, thermal, electromagnetic, indoor lighting, etc. to power SNs [17,18]. In this case, sensor nodes are equipped with rechargeable batteries which are charged up by the energy sources through a recharging circuitry. Although renewable energy sources significantly prolong the lifetime of an SN, their usage gives rise to the question of how to handle the variable energy level in its battery intelligently so that the SN can maintain its functionality perpetually. We consider in this thesis the architecture depicted in Figure 1.1 in which individual sensor nodes directly communicate with a sink node in a single-hop network which acts as a gateway to the Internet and focus on how to manage the energy of an individual node.

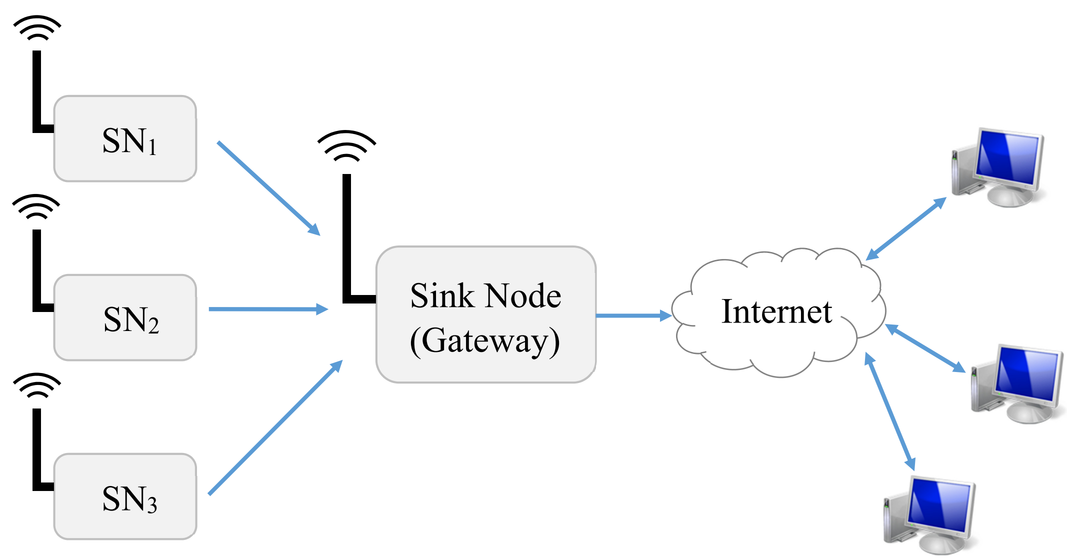

Figure 1.1: Wireless sensor nodes connected to the Internet via the sink node which serves as a gateway.

1.2 Related Work

In this section, we summarize the related work in the literature on the energy management strategies proposed for energy harvesting wireless sensor nodes and also the statistical methods used for modeling energy harvesting processes.

1.2.1 Energy Management in Energy Harvesting Wireless Sensor Nodes

There have been quite a few recent studies on the energy management problem in energy harvesting wireless sensor nodes, see [19] for a recent review. A subset of these studies concentrate on an optimization problem on the basis of the availability of the offline knowledge of energy and data arrivals at the SN, which is most commonly referred to as the *offline* problem in the literature. The authors in [20] examine two cases: (i) all packets are ready to be transmitted before the system is initialized and (ii) packets arrive after system start-up. In both cases, energy and data packet sizes and arrival times are known prior to the start of the transmissions and the main objective is to minimize the transmission completion time. [21] seeks to maximize the throughput in a given deadline, while assuming a time-varying capacity and leakage for the battery. Moreover, instead of energy quanta arrivals, the model in [21] also considers continuous energy profiles, which are again known in advance. [22] examines the optimal solution that maximizes the throughput for the offline scenario where due to storage losses, some portion of the available energy is lost while being stored to the battery. First showing that the optimal offline policy has a two-threshold structure, the authors then provide a water-filling algorithm for the fading channel case and finally a dynamic program formulation for an online policy is proposed.

As opposed to the *offline* problem; in *online* setting, energy and/or data packets arrive at the system according to statistical models. In [23], the authors establish a threshold policy to maximize an average long-term reward function for an energy harvesting process modelled as a two-state Markov chain; whereas in [24], a new dimension which represents the number of packets queued in a data buffer is added to the Markov chain. [25] proposes a stochastic scheduling mechanism to sense the environment with high probability if the probability that a significant change has occurred in the environment is also high, where the changes in the state of the environment are predicted by using statistical models. Another change detection process is examined in [26] in which power allocation and detection schemes are designed in order to minimize the detection delay while the battery is replenished by a random process. [27] seeks to solve an optimization problem to obtain sensing and transmission policies with the problem constraints being the probabilities that the data buffer gets full or the battery depletes. Another example that manages data and energy buffers simultaneously is [28], in which transition decisions between sleep and wake states are made according to a cost function that takes into account the levels of these buffers. In [29], energy reserve in a sensor node is assumed to be partially known and by comparing the energy level with a predetermined threshold, the controller makes sensing decisions.

A very commonly used sensing policy in SNs is *duty cycling*, in which a sensor node "wakes up" at certain times to measure data and then transits into a "sleep" state in order to prevent unnecessary energy consumption [30]. Adaptive duty cycling is a widespread online energy management strategy proposed in the literature to balance energy consumption during data measurement/transmission and the randomness of the renewable energy resources [31–35]. The authors in [31] consider several energy storage (rechargeable battery, capacitor) and energy harvesting models (predictable, stochastic) for which optimal energy spending algorithms that maximize the data rate of a single node are proposed. In [32], the authors formulate an optimization problem to obtain the optimal duty cycle, where the constraints are the QoS regarding latency and loss probability of the packets that are queued in a finite-size buffer before being transmitted. The authors in [33] compare two policies that adjust sensing epochs and make sensing decisions. In the first policy, sensing events are periodic and take place if there is enough energy in the battery or otherwise skipped, which is the optimal policy for an infinite-size battery whereas in the second policy, time between two consecutive sensing events also depends on the battery level and is adjustable. [34] addresses the problem from a control-theoretic perspective not only to adjust the duty cycle but also to decrease its variance for sustaining the stability of this parameter. The study in [35] uses a discrete model as the estimate of the harvested energy, which is assumed to be periodic. Duty cycles are initialized according to the levels of this discrete model. Moreover, according to the deviations of the actual energy from the estimate, duty cycles are adjusted online.

Figure 1.2 depicts the system diagram we envision in this thesis. While an energy harvesting resource provides power to the rechargeable battery, the SN measures the physical quantities of interest from the environment and transmits data packets containing information regarding the measured data directly to the sink node in a single-hop manner during which energy is depleted from the battery. In this model, we use stochastic models to characterize the energy harvesting process which will be discussed in the following section in detail. As in the studies in [31–35], we focus on the frequency of sensing events and specifically its effects on the system performance and probability that the battery of SN is depleted within a given amount of time. In particular, we model the duty cycle of the SN as an exponentially distributed random variable whose rate determines the frequency of the data from the environment. We will refer to this rate as *sensing rate* throughout this thesis. Obviously, more frequent data gathering (i.e., higher sensing rate) will improve the performance of the system of interest at the risk of depleting the energy stored in the battery more rapidly. This particular tradeoff between performance and lifetime is the main focus of this thesis.

1.2.2 Models for Energy Harvesting Processes

Due to the random and intermittent nature of energy harvesting resources, energy harvesting processes (EHPs) are commonly modeled by stochastic processes in the literature. [29, 36–48]. In [29, 36–44], discrete Markov models are used to model the EHP. In [45], energy "packets" are assumed to arrive at the system according

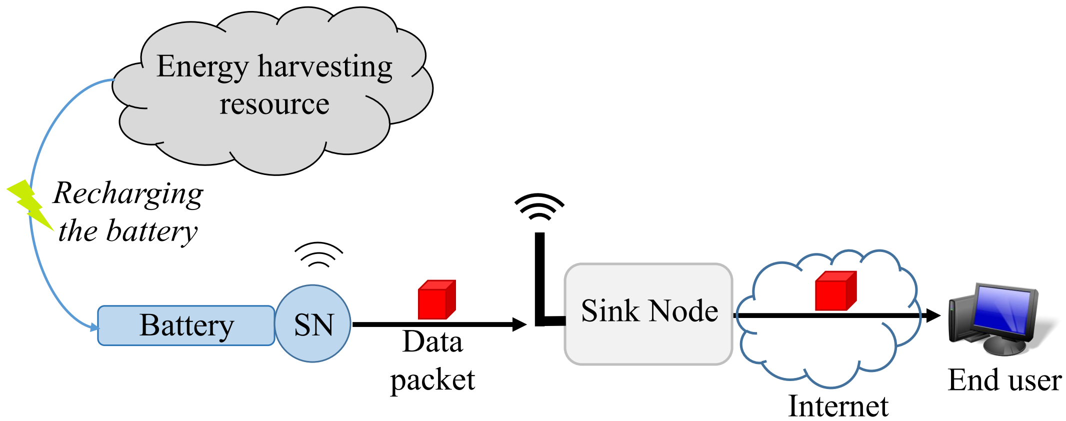

Figure 1.2: System diagram.

to a Poisson process. [46] investigates how well six types of distributions, namely discrete uniform, geometric, transformed geometric, Poisson, transformed Poisson and two-state discrete Markovian, fit to the real-world solar data. Continuous time Markov Chain (CTMC) models of the EHP are studied in [47, 48]. Similar to these studies, we propose in this thesis to use CTMC-based EHPs.

In this thesis, we envision an energy harvesting SN model illustrated in Figure 1.3 with its rechargeable battery modeled by a single buffer for energy storage. The EHP $Z(t)$ dictates the instantaneous rate at time t at which the battery is charged/discharged. Positive (negative) values for this rate are representative of energy harvesting (leakage). We assume that $Z(t)$ is governed by a general finite-state CTMC with an initial probability vector $\boldsymbol{\alpha}$ at time zero. In the SN model of Figure 1.3, the process $X(t) \in [0, B]$ denotes the stored energy at the battery at time t and the capacity limit B represents the maximum amount of energy that the battery can hold. The initial battery level is denoted by u, i.e., $X(0) = u$. Similar to the system model envisioned in [23] and [26], when the SN decides to sense the environment, it samples the physical quantities of interest, processes this information, forms a data packet, and immediately transmits it towards the receiver using the WSN facilities. Since the sensing, processing, packetization, and transmission sub-steps are combined into one single step in this model, the system we envision does not need to possess a data buffer to store data packets. For simplicity, we call this combined step as *sensing*. The count process related to the sensing epochs (or the data packet arrival process) is modeled by a non-homogenous Poisson process with rate $\lambda(X(t), Z(t))$, also called the adaptive sensing rate, which is allowed to depend on the instantaneous battery level and the state of the harvester process. For the purpose of analytical tractability, we assume that the SN does not carry transit traffic and the transmitted packets are not errored in transit. Study of systems involving routed WSN traffic and wireless packet errors are left for future research. These assumptions are more in line with low-power wide area IoT networks as opposed to lower range wireless multi-hop sensor networks. Moreover, the energy dissipated for one single data packet transmission (denoted by S) is assumed to be exponentially distributed with mean $E[S]$. We assume that this quantity captures the energy dissipated for all the four sub-steps. Since the time scales of operation for the slower EHP and the relatively rapid packet transmission process are quite different, we assume for the sake of simplicity that the packet transmission takes place instantaneously resulting in an abrupt energy drop by an amount of S each time a data packet gets to be transmitted. Battery outage is said to occur at time t when the buffer is first depleted, i.e., $X(t) = 0$, after which the SN would not able to fulfill its functionalities. As the QoS constraint, we focus in this thesis on the lifetime of the battery and propose to use the finite-horizon battery outage probability which is defined as the probability of battery outage within a given time horizon H. The main goal of this thesis is to first analytically obtain the finite-horizon battery outage probability as a function of all system model parameters. Note that this probability depends on the initial buffer level u, initial probability vector $\boldsymbol{\alpha}$ of the EHP, and also the time horizon H. The second goal of this thesis is to use this mathematical analysis as an instrument to find the optimal transmission policies regarding the choice of the sensing rate function $\lambda(X(t), Z(t))$ meeting the lifetime constraint with the purpose of maximizing the average long-term sensing rate. Towards the second goal and for tractability purposes, we focus our attention to the very commonly used two-state CTMC model for the EHP and threshold-based transmission policies in which the instantaneous sensing rate λ is either λ_{min} or $\lambda_{max} > \lambda_{min}$, depending on whether $X(t)$ is above or below a given threshold dictated by the current state of the harvesting process. This generality in analysis allows us to compare and contrast various non-adaptive/adaptive

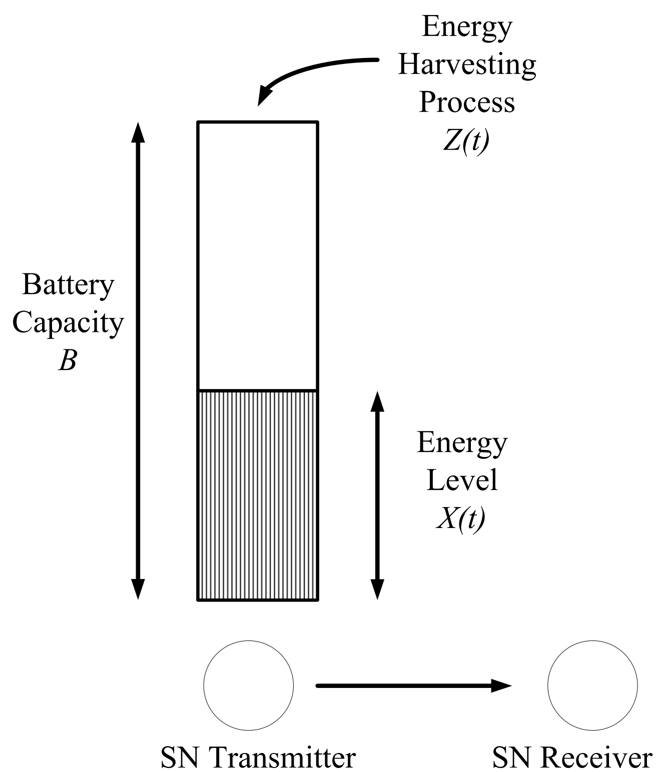

Figure 1.3: Energy harvesting SN model.

sensing rate policies.

For mathematical analysis, a connection is established in this thesis between ruin probabilities in risk theory and battery outage probabilities in energy harvesting sensor nodes. In risk theory, the ruin problem is described through an insurance company which is exposed to an incoming cash flow in the form of premiums and an outgoing cash flow in the form of claims, the arrival epochs and sizes of claims being modeled by various stochastic processes in the literature; see [49] and the references therein. For an insurer with initial surplus u, the ultimate ruin probability is the probability that the insurer's surplus level eventually falls below zero, i.e., the insurance company goes bankrupt [49]. In most practical scenarios, it is crucial to know about the probability of the surplus level falling below zero within a given finite time horizon, called the finite-horizon ruin probability [50]. The role of premiums (claims) in risk theory will be shown in this thesis to be played by energy harvesting (sensing) in energy harvesting sensor nodes. Consequently, the counterpart of ruin probabilities turns out to be battery outage probabilities, both within a given time horizon. Recently, [51] proposed a Multi-Regime Markov Fluid Queue (MRMFQ) model to find the finite-horizon ruin probabilities for an insurance company with surplus-dependent premiums, claim arrivals modeled by a Markovian arrival process, and PH-type claim sizes with a matrix-analytical algorithm. With the proposed technique of [51], one can express the finite-horizon ruin probability in terms of the steady-state probability mass accumulations of the associated MRMFQ at certain levels. In this thesis, we extend the method proposed in [51] to compute the finite-horizon battery outage probabilities of Figure 1.3 using the so-called risk-theoretic MRMFQ model. As related work, Markov fluid queue models have been used to analyze the energy process of a rechargeable battery in a few studies. In [52], a two-regime fluid queue is used where the regimes correspond to the battery level compared to a threshold and battery discharge rates are chosen to be different in these two regimes. On the other hand, [53] investigates a wireless node powered by multiple batteries each of which is modeled by an MRMFQ but the focus has been on the mean SN lifetime rather than the battery outage probability, the latter being more information-bearing.

The contributions of this thesis can be summarized as follows:

- A risk-theoretic methodology is proposed to calculate the finite-horizon battery outage probability of an energy harvesting wireless sensor node that employs threshold-based adaptive sensing rate policies. Simulation results verify that the proposed method can very rapidly and accurately calculate the finite-horizon battery outage probability and average sensing rate. To the best of our knowledge, such a numerical method to calculate the battery outage probability within a given finite lifetime does not exist in the literature.

- By using this analytical tool as a numerical engine, we propose a search-based method to find the optimal operational parameters of a threshold-based sensing policy, namely State-Dependent Threshold Policy (SDTP), that maximizes the average sensing rate while lifetime constraints are satisfied.

The thesis is organized as follows. In Chapter II, we describe two types of Markov Fluid Queues, namely Single Regime Markov Fluid Queues (SRMFQs) and Multi Regime Markov Fluid Queues (MRMFQs). We also provide the boundary conditions and equations required to solve each of them and then describe the procedure to solve the latter in detail. The computational procedure for finding the battery outage probabilities for the system of Figure 1.3 is presented in Chapter III. In Chapter IV, the proposed analytical technique is validated using simulations. Moreover, the engineering methodology that we propose is presented for a wide range of system parameters. In Chapter V, we conclude the thesis with final remarks.

Chapter 2

Markov Fluid Queues

Markov Fluid Queues (MFQs) are systems in which the rate of change of a buffer content is governed by a Markov Process, which is usually called the *background process* or *driving process*. This process is a CTMC whose states determines the rates of change (or *drifts*) of the buffer content. Hence, MFQs have two key components, the infinitesimal generator of the background process and the drift values for each state of this process.

Dividing the buffer into fixed-size *regimes* expands the scope of the analysis that can be done using MFQs. With different numbers of regimes, three different systems can be derived from MFQs: Single-Regime MFQ (SRMFQ), Multi-Regime MFQ (MRMFQ) and Continuous Feedback MFQ (CFMFQ).

In SRMFQs, the background process and drift values are fixed and independent of the buffer content. On the other hand, these parameters are piecewise constant (continuous) functions of the buffer level in MRMFQs (CFMFQs). In this chapter, after briefly describing SRMFQs, we discuss MRMFQs, which will be used in the analytical method proposed in this thesis, in detail.

MFQs have been studied in several studies including [54], [55], [56], [57], [58]. In [54], the main focus is on SRMFQs and a spectral solution approach is used to solve for the steady-state behavior of the system which is also utilized by [55] to solve multi-regime systems. The study in [56] proposes a stable numerical method to solve the steady-state joint probability density function (pdf) vector of SRMFQs which is based on Additive Decomposition (AD), whereas [57] extends this method to multi-regime case. We will utilize the numerical method described in [57] to obtain the steady-state solution of the MRMFQ model proposed in this thesis.

2.1 Single-Regime Markov Fluid Queues

Let $X(t)$ and $Z(t)$ denote the buffer content and the background process, respectively, at time t. Moreover, let Q denote the infinitesimal generator of $Z(t)$. For N being the number of states of $Z(t)$, we also denote the drift of each state by r_i, for $1 \leq i \leq N$. The diagonal drift matrix R which contains the drift values on the diagonal is defined as follows:

$$R = \begin{bmatrix} r_1 & & & \\ & r_2 & & \\ & & \ddots & \\ & & & r_N \end{bmatrix}.$$

We also define S_0, S_- and S_+ as the sets of states with zero, negative and positive drifts, respectively. The solution of an SRMFQ for a finite buffer of size B is expressed either in terms of the probability density function (pdf) or the cumulative density function (cdf) of the queue occupancy at the steady-state. The cdf and pdf vectors of an SRMFQ are defined as follows:

$$\begin{aligned} F_i(x,t) &= Pr\{X(t) \leq x,\ Z(t) = i\}, && 1 \leq i \leq N, \\ F(x,t) &= \left[F_1(x,t) \cdots F_N(x,t)\right], && 0 < x < B, \\ f_i(x,t) &= \tfrac{d}{dx} F_i(x,t), && 1 \leq i \leq N, \\ f(x,t) &= \left[f_1(x,t) \cdots f_N(x,t)\right], && 0 < x < B. \end{aligned}$$

Then the steady-state cdf are pdf vectors can be written as:

$$
\begin{aligned}
F_i(x) &= \lim_{t\to\infty} F_i(x,t), && 1 \le i \le N,\\
F(x) &= \left[F_1(x) \cdots F_N(x)\right], && 0 < x < B,\\
f_i(x) &= \lim_{t\to\infty} f_i(x,t), && 1 \le i \le N,\\
f(x) &= \left[f_1(x) \cdots f_N(x)\right], && 0 < x < B.
\end{aligned}
$$

The steady-state joint pdf vector $f(x) = [f_1(x) \cdots f_N(x)]$, $0 \le x \le B$, where B is a finite buffer size, is given by the following system of differential equations:

$$\frac{d}{dx} f(x)R = f(x)Q \tag{2.1}$$

with the probability mass accumulations occurring at the boundary points 0 and B denoted by $c^{(0)} = \left[c_1^{(0)} \cdots c_N^{(0)}\right]$ and $c^{(B)} = \left[c_1^{(B)} \cdots c_N^{(B)}\right]$, respectively, and given by as follows:

$$
\begin{aligned}
c_i^{(0)} &= \lim_{t\to\infty} Pr\{X(t) = 0,\ Z(t) = i\}, \quad 1 \le i \le N,\\
c_i^{(B)} &= \lim_{t\to\infty} Pr\{X(t) = B,\ Z(t) = i\}, \quad 1 \le i \le N,
\end{aligned}
$$

for $i = 1, 2, ..., N$. The steady-state solution of a SRMFQ should satisfy the following boundary conditions:

$$c_i^{(0)} = 0, \quad \forall i \in S_+, \tag{2.2}$$

$$c_i^{(B)} = 0, \quad \forall i \in S_-, \tag{2.3}$$

$$f(0+)R = c^{(0)}\tilde{Q}^{(0)}, \tag{2.4}$$

$$f(B-)R = c^{(B)}\tilde{Q}^{(B)}, \tag{2.5}$$

$$\left(\int_0^B f(x)dx + c^{(0)} + c^{(B)}\right)\mathbf{1} = 1, \tag{2.6}$$

where $\tilde{Q}^{(0)}$ and $\tilde{Q}^{(B)}$ are the infinitesimal generator matrices defined at the boundary points 0 and B, respectively, and $\mathbf{1}$ denotes a column vector of ones of appropriate size. If the buffer size is infinity, condition (2.3) is replaced with

$c^{(B)} = [0 \cdots 0]$ since there can be no accumulation at infinity; and (2.5) is replaced with stability conditions so that the buffer content will not increase indefinitely. Since SRMFQs are equivalent to MRMFQs with the regime number being equal to one, their steady-state pdf solution can directly be obtained from the one of MRMFQs, which will be described next. For the details of SRMFQ boundary and stability conditions, the reader is referred to [59].

2.2 Multi-Regime Markov Fluid Queues

The main difference between SRMFQs and MRMFQs is that the generator and drift matrices in an MRMFQ system are piecewise constant functions of the buffer level. Having a finite size $B < \infty$, the buffer is partitioned into K regimes, where $K > 1$, with the regime boundaries ordered as $0 = T^{(0)} < T^{(1)} < ... < T^{(K-1)} < T^{(K)} = B$. If the buffer size is infinity, than the size of the last regime will be infinity as well.

If $T^{(k-1)} < X(t) < T^{(k)}$, the system is said to be in regime k at time t. We denote infinitesimal generator and drift matrices of regime k by $Q^{(k)}$ and $R^{(k)}$, respectively, for $1 \leq k \leq K$, where $R^{(k)}$ is the diagonal matrix whose diagonal elements are the drifts of state i, $r_i^{(k)}$, for $1 \leq i \leq N$. Note that within regime k, $Q^{(k)}$ and $R^{(k)}$ are constant. Similar to $Q^{(k)}$ and $R^{(k)}$, we define $\tilde{Q}^{(k)}$ and $\tilde{R}^{(k)}$ as the infinitesimal generator and drift matrices associated with the boundary point $T^{(k)}$ for $0 \leq k \leq K$, where the drift of state i at the boundary $T^{(k)}$ is denoted by $\tilde{r}_i^{(k)}$. $S_0^{(k)}$, $S_-^{(k)}$ and $S_+^{(k)}$ denote the sets of states with zero, negative and positive drifts, respectively, in regime k. On the boundary point $T^{(k)}$, $0 \leq k \leq K$, these sets are denoted by $\tilde{S}_0^{(k)}$, $\tilde{S}_-^{(k)}$ and $\tilde{S}_+^{(k)}$. According to the signs of the drifts of a state in two adjacent regimes, the states with non-zero drifts are classified into three as follows:

- *Absorbing state*: If $r_i^{(k)} > 0$ and $r_i^{(k+1)} < 0$, state i is called *absorbing* at the boundary point $T^{(k)}$.

- *Repulsive state*: If $r_i^{(k)} < 0$ and $r_i^{(k+1)} > 0$, state i is called *repulsive* at the boundary point $T^{(k)}$.

- *Emitting state*: If $r_i^{(k)}$ and $r_i^{(k+1)}$ have the same sign, state i is called *emitting* at the boundary point $T^{(k)}$.

We also define joint cdf and pdf vectors for regime k, $1 \leq k \leq K$, as follows:

$$
\begin{aligned}
F_i^{(k)}(x,t) &= Pr\{X(t) \leq x,\ Z(t) = i\}, && 1 \leq i \leq N, \\
F^{(k)}(x,t) &= \left[F_1^{(k)}(x,t) \cdots F_N^{(k)}(x,t)\right], && T^{(k-1)} < x < T^{(k)}, \\
f_i^{(k)}(x,t) &= \tfrac{d}{dx} F_i^{(k)}(x,t), && 1 \leq i \leq N, \\
f^{(k)}(x,t) &= \left[f_1^{(k)}(x,t) \cdots f_N^{(k)}(x,t)\right], && T^{(k-1)} < x < T^{(k)}.
\end{aligned}
$$

Then steady-state cdf and pdf vectors can be written as:

$$
\begin{aligned}
F_i^{(k)}(x) &= \lim_{t \to \infty} F_i^{(k)}(x,t) && 1 \leq i \leq N, \\
F^{(k)}(x) &= \left[F_1^{(k)}(x) \cdots F_N^{(k)}(x)\right] && T^{(k-1)} < x < T^{(k)}, \\
f_i^{(k)}(x) &= \lim_{t \to \infty} f_i^{(k)}(x,t) && 1 \leq i \leq N, \\
f^{(k)}(x) &= \left[f_1^{(k)}(x) \cdots f_N^{(k)}(x)\right] && T^{(k-1)} < x < T^{(k)}.
\end{aligned}
$$

Moreover, the steady-state probability mass accumulations are defined at boundary point k for $0 \leq k \leq K$ as follows:

$$
\begin{aligned}
c_i^{(k)} &= \lim_{t \to \infty} Pr\{X(t) = 0,\ Z(t) = i\}, && 1 \leq i \leq N, \\
c^{(k)} &= \left[c_1^{(k)} \cdots c_N^{(k)}\right], && 1 \leq i \leq N.
\end{aligned}
$$

Similar to the Eqn. (2.1), the set of differential equations that give the steady-state solution of an MRMFQ in terms of joint pdf vector is as follows:

$$
\frac{d}{dx} f^{(k)}(x) R^{(k)} = f^{(k)}(x) Q^{(k)}. \tag{2.7}
$$

The steady-state solution given by Eqn. (2.7) should satisfy the following boundary conditions:

$$c_i^{(0)} = 0, \quad \forall i \in S_+^{(1)}, \tag{2.8}$$

$$c_i^{(k)} = 0, \quad \forall i \in \left(S_+^{(k)} \cap S_+^{(k+1)}\right) \cup \left(S_-^{(k)} \cap S_-^{(k+1)}\right), \quad 1 \leq k < K, \tag{2.9}$$

$$c_i^{(k)} = 0, \quad \forall i \in \left(S_-^{(k)} \cap S_+^{(k+1)}\right) \cap \left(\tilde{S}_+^{(k)} \cup \tilde{S}_-^{(k)}\right), \quad 1 \leq k < K, \tag{2.10}$$

$$c_i^{(K)} = 0, \quad \forall i \in S_-^{(K)}, \tag{2.11}$$

$$f^{(1)}(0+)R^{(1)} = c^{(0)}\tilde{Q}^{(0)}, \tag{2.12}$$

$$f^{(k+1)}(T^{(k)}+)R^{(k+1)} - f^{(k)}(T^{(k)}-)R^{(k)} = c^{(k)}\tilde{Q}^{(k)}, \quad 1 \leq k < K, \tag{2.13}$$

$$f_i^{(k)}(T^{(k)}-) = 0, \quad \forall i \in S_-^{(k)} \cap \left(\tilde{S}_0^{(k)} \cup \tilde{S}_+^{(k)}\right), \quad 1 \leq k < K, \tag{2.14}$$

$$f_i^{(k+1)}(T^{(k)}+) = 0, \quad \forall i \in \left(\tilde{S}_0^{(k)} \cup \tilde{S}_-^{(k)}\right) \cap S_+^{(k+1)}, \quad 1 \leq k < K, \tag{2.15}$$

$$f^{(K)}(B-)R^{(K)} = -c^{(K)}\tilde{Q}^{(K)}, \tag{2.16}$$

$$\left(\sum_{k=1}^{K} \int_{T^{(k-1)}+}^{T^{(k)}-} f^{(k)}(x)dx + \sum_{k=0}^{K} c^{(k)} \right) \mathbf{1} = 1. \tag{2.17}$$

Note that the boundary conditions (2.11) and (2.16) are valid only if the buffer is of finite size. On the other hand, if $B = \infty$, $a_0^{(K)} = 0$ and $a_+^{(K)} = \mathbf{0}$ should hold since the system must be bounded in regime K, which replace the conditions (2.11), (2.16). Moreover, the stability condition

$$\pi^{(K)}R^{(K)}\mathbf{1} < 0 \tag{2.18}$$

should also be satisfied where $\pi^{(K)}$ is the steady-state vector of $Q^{(K)}$.

2.3 Ordered Schur Form

Before outlining the numerical methodology used in thesis, we first describe the ordered Schur decomposition of a given matrix, which will be a significant component of the methodology. In particular, our aim in this section is to find a matrix Y for a real square matrix A such that

$$Y^{-1}AY = \begin{bmatrix} A_0 & & \\ & A_- & \\ & & A_+ \end{bmatrix}, \tag{2.19}$$

where A_0, A_- and A_+ are upper triangular blocks having eigenvalues with 0, negative and positive real parts on the diagonals, respectively.

Theorem 1. *There exists an orthogonal matrix Z for every real square matrix A such that*

$$Z^T AZ = T = \begin{bmatrix} T_{11} & T_{12} \\ 0 & T_{22} \end{bmatrix},$$

where T is upper block-triangular with each diagonal block being either a 1×1 entry and an eigenvalue of A or a 2×2 matrix corresponding to a complex conjugate pair of eigenvalues of A. Moreover, matrix Z can be chosen in a way that the eigenvalues are placed in the diagonal blocks of T in any desired order [60].

By Theorem 1, one can find a matrix Z such that

$$Z^T AZ = \begin{bmatrix} A_0 & A_1 & A_2 \\ & A_- & A_3 \\ & & A_+ \end{bmatrix},$$

where A_0, A_- and A_+ are upper triangular blocks as (2.19). In order to obtain the exact form in (2.19), the authors in [61] describes a procedure which defines matrix Y as follows:

$$Y = Z \begin{bmatrix} I & X_1 \\ 0 & I \end{bmatrix} \begin{bmatrix} I & 0 & 0 \\ 0 & I & X_2 \\ 0 & 0 & I \end{bmatrix},$$

where X_1 and X_2 can be obtained by solving the following Sylvester equations:

$$X_1 \begin{bmatrix} A_- & A_3 \\ 0 & A_+ \end{bmatrix} - A_0 X_1 = \begin{bmatrix} A_1 & A_2 \end{bmatrix}, \tag{2.20}$$

$$X_2 A_+ - A_- X_2 = A_3. \tag{2.21}$$

2.3.1 Matlab Implementation

Let us now present a numerical example to demonstrate how to obtain the ordered Schur form by using MATLAB version 8.5. We consider a 4-state CTMC with the following infinitesimal generator and drift matrices:

$$Q = \begin{bmatrix} -3 & 0.5 & 1 & 1.5 \\ 1 & -1.5 & 0.5 & 0 \\ 0 & 2 & -2 & 0 \\ 1 & 3 & 0.5 & -4.5 \end{bmatrix}, \; R = \begin{bmatrix} 1 & 0 & 0 & 0 \\ 0 & -2 & 0 & 0 \\ 0 & 0 & -1 & 0 \\ 0 & 0 & 0 & 3 \end{bmatrix},$$

from which matrix A is computed as[1]:

$$A = Q(R)^{-1} = \begin{bmatrix} -3 & -0.25 & -1 & 0.5 \\ 1 & 0.75 & -0.5 & 0 \\ 0 & -1 & 2 & 0 \\ 1 & -1.5 & -0.5 & -1.5 \end{bmatrix}.$$

In MATLAB , the Schur decomposition of matrix A is obtained by executing the command `[Z1,T1]=schur(A)`, which gives an orthogonal matrix Z_1 and upper block-triangular matrix T_1 as:

$$Z_1 = \begin{bmatrix} -0.7697 & 0.5494 & -0.3112 & 0.0941 \\ 0.1955 & -0.2660 & -0.8028 & 0.4965 \\ 0.0370 & -0.0821 & -0.4974 & -0.8628 \\ 0.6066 & 0.7878 & -0.1059 & 0.0121 \end{bmatrix},$$

[1]One can follow the procedure described in [57] to handle the case of singular per-regime drift matrices which is caused by zero-drift states.

$$
T_1 = \begin{bmatrix} -3.2825 & 0.8147 & -0.5633 & -0.4066 \\ 0 & -0.8713 & 2.0846 & 0.0107 \\ 0 & 0 & 0 & 0.2658 \\ 0 & 0 & 0 & 2.4038 \end{bmatrix},
$$

which satisfy the matrix equation $Z_1^T A Z_1 = T_1$. We note that the eigenvalues of A are -3.2825, -0.8713, 0 and 2.4038, which occur in the diagonal of matrix T_1. In order to place the eigenvalues in specific locations, we the function `ordschur.m` in MATLAB that takes an input vector for ordering the eigenvalues, highest (lowest) value of which corresponds to the leftmost (rightmost) block diagonal. For this particular example, we execute the following command:

```
Z,T = ordschur(Z1,T1,[2 2 3 1])
```

to place the zero eigenvalue to the upper-left corner, followed by the blocks containing the eigenvalues with negative real parts and then the ones with positive real parts. At this step, we have the orthogonal matrix Z satisfying

$$
Z^T A Z = T = \begin{bmatrix} 0 & 0.5344 & 1.9235 & 0.0456 \\ 0 & -3.2825 & 1.1580 & 0.4193 \\ 0 & 0 & -0.8713 & 0.2411 \\ 0 & 0 & 0 & 2.4038 \end{bmatrix}.
$$

As discussed before, we now eliminate the non-zero entries in the off-diagonals. We solve two Sylvester matrix equations for matrices X_1 and X_2, which are used to eliminate the non-zero off-diagonal entries in the first and second-third rows, respectively, by executing the following commands:

```
X1 = −T(1,2:4)/T(2:4,2:4),                        (2.22)
X2 = sylvester(−T(2:3,2:3),−T(4,4),T(2:3,4)).     (2.23)
```

We finally calculate matrix Y as

$$Y = Z \begin{bmatrix} I & -X_1 \\ 0 & I \end{bmatrix} \begin{bmatrix} I & 0 & 0 \\ 0 & I & -X_2 \\ 0 & 0 & I \end{bmatrix},$$

$$= \begin{bmatrix} 0.2582 & 0.7798 & -1.1249 & 0.1555 \\ -0.5164 & -0.1980 & 0.6136 & 0.3741 \\ -0.2582 & -0.0375 & 0.1986 & -0.9265 \\ 0.7746 & -0.6146 & -2.2791 & 0.0147 \end{bmatrix},$$

which satisfies

$$Y^{-1}AY = \begin{bmatrix} 0 & 0 & 0 & 0 \\ 0 & -3.2825 & 1.1580 & 0 \\ 0 & 0 & -0.8713 & 0 \\ 0 & 0 & 0 & 2.4038 \end{bmatrix}.$$

2.4 Solution of MRMFQs

Throughout the thesis, we assume that per-regime drift matrices $R^{(k)}$, $k = 1, ..., K$ are nonsingular because all of the drift values of the model proposed in the next chapter are non-zero. Hence, the solution provided in this section covers the steps for the case where per-regime drift matrices are invertible. Nonetheless, the reader is referred to [57] for the details of the solution procedure for the case with zero drift states.

First, we define $A^{(k)} = Q^{(k)} \left(R^{(k)}\right)^{-1}$ for $k = 1, ..., K$ from which Eqn. (2.7) can be written as follows:

$$\frac{d}{dx} f^{(k)}(x) = f^{(k)}(x) A^{(k)}. \tag{2.24}$$

As a direct consequence of Theorem 1 and the remaining steps in Section 2.3, one can find a non-singular matrix $Y^{(k)}$ for matrix $A^{(k)}$ such that the form in (2.19) is obtained. In mathematical form, for $k = 1, ..., K$, one can write the following expression:

$$\left(Y^{(k)}\right)^{-1} AY^{(k)} = \begin{bmatrix} \mathbf{0} & & \\ & A_-^{(k)} & \\ & & A_+^{(k)} \end{bmatrix} \tag{2.25}$$

where eigenvalues of matrix $A^{(k)}$ with negative and positive real parts appear on the diagonals of $A_-^{(k)}$ and $A_+^{(k)}$, respectively; and $\mathbf{0}$ is a square matrix having zeros on the diagonal whose size is equal to the number of zero eigenvalues of matrix $A^{(k)}$. We now decompose matrix $\left(Y^{(k)}\right)^{-1}$ as

$$\left(Y^{(k)}\right)^{-1} = \begin{bmatrix} L_0^{(k)} \\ L_-^{(k)} \\ L_+^{(k)} \end{bmatrix} \tag{2.26}$$

where the blocks $L_0^{(k)}$, $L_-^{(k)}$ and $L_+^{(k)}$, correspond to the zero eigenvalues and the ones with negative and positive real parts, respectively. Then, the solution of (2.7) for regime k, $k = 1, ..., K$ can be written as follows:

$$f^{(k)} = a^{(k)} \begin{bmatrix} L_0^{(k)} \\ e^{A_-^{(k)}\left(x - T^{(k-1)}\right)} L_-^{(k)} \\ e^{-A_+^{(k)}\left(T^{(k)} - x\right)} L_+^{(k)} \end{bmatrix} \tag{2.27}$$

where $a^{(k)} = \begin{bmatrix} a_0^{(k)} & a_-^{(k)} & a_+^{(k)} \end{bmatrix}$ is the vector of unknowns to be solved for. Finally, one can solve for the unknowns $a^{(k)}$ and $c^{(k)}$ by re-writing equations (2.8)-(2.17) (using Eqn. (2.27)) in terms of the unknowns. This algorithm requires the solution of a linear matrix equation of at most size $N(2K + 1)$. The computational complexity of the proposed algorithm can be reduced to $\mathcal{O}(N^3K)$ on the basis of the observation that the linear matrix equation is in block tridiagonal form [51].

Chapter 3

Fluid Queue-Based Analysis of Energy Harvesting Sensor Nodes

In this chapter, we combine the energy process of an energy harvesting SN with the fluid queue analysis described in Chapter 2. We construct the system model and then, we derive the expressions for the finite-horizon battery outage probability and average sensing rate.

3.1 System Model

Without loss of generality, we assume that an SN consumes energy only when it transmits packets. There are also studies that examines the case in which an SN consumes energy also during processing the data and when it is idle. Idle state power can be modeled by a negative drift for the states in which the SN is idle. Furthermore, energy required for data processing can simply be combined with the consumed energy during transmission since there is no buffer for data storage and all the measured data and corresponding data packets are transmitted immediately as long as there is enough energy in the battery.

Table 3.1: Table of main notation.

Parameter	Definition	Unit
$X(t)$	Battery level at time t	mWh
u	Initial battery level ($X(0)$)	mWh
B	Battery capacity	mWh
p_i	Energy harvester output power at state i	mW
d_i	Net drift of the battery at state i	mW
l_b	Energy leakage rate of the battery	mW
$\lambda_i(k)$	Sensing rate at state i and regime k	hour^{-1}
$\boldsymbol{\alpha}$	Initial probability vector	
H	Deterministic time horizon	hour
l	Erlangization level of the horizon H	

For tractability of the model, we recapitulate the main notation in Table 3.1. The Energy Harvesting Process (EHP) $Z(t) \in \{0, 1, ..., N-1\}$ is governed by an N-state CTMC with infinitesimal generator denoted by Q. We refer to the states of the energy harvesting process as the *harvester states*. When the EHP resides in state i, the harvester output power level is denoted by p_i, for $0 \leq i \leq N-1$. Accordingly, we define the matrix $P = \mathbf{diag}(p_0, p_1, \ldots, p_{N-1})$. A fixed leakage rate from the battery is assumed and denoted by l_b. Subsequently, we define the net power matrix $D = P - l_b\mathbf{I} = \mathbf{diag}(d_0, d_1, \ldots, d_{N-1})$, where $d_i = p_i - l_b$ denotes the net rate of change of the stored energy in the battery when the EHP resides in state i.

We focus on the particular case when the sensing rate function $\lambda(X(t), Z(t)$ is a piece-wise constant function of the instantaneous battery level $X(t)$, i.e., the sensing rate is fixed when $X(t)$ resides between two boundaries. For this purpose, we define the regime boundaries $0 = T^{(0)} < T^{(1)} < \cdots < T^{(J)} = u < \cdots < T^{(K)} = B$, where u and B are the initial battery level and battery capacity, respectively. The battery is said to reside in regime k at time t when $T^{(k-1)} < X(t) < T^{(k)}$. We denote the sensing rate in harvester state i and regime k by $\lambda_i(k)$ for $0 \leq i \leq N-1$ and $1 \leq k \leq K$. We define the regime-k sensing rate matrix $\Lambda(k) = \mathbf{diag}\left(\lambda_0(k), \lambda_1(k), \ldots, \lambda_{N-1}(k)\right)$ for $1 \leq k \leq K$.

The system starts to operate with initial battery level u and in an harvester state according to a given initial probability vector $\boldsymbol{\alpha} = [\alpha_0\ \alpha_1\ \ldots\ \alpha_{N-1}]$ where

$\alpha_i = \Pr\{Z(0) = i\}$. Whenever $Z(t)$ is in state i, energy is stored in the battery with rate $d_i = p_i - l_b$. When $p_i < l_b$, the energy buffer is drained at rate $l_b - p_i$. When $T^{(k-1)} < X(t) \leq T^{(k)}$, a sensing event occurs in the interval $(t, t + \Delta t)$ with probability $\lambda_i(k)\Delta(t) + o(\Delta t)$ where $\frac{o(\Delta t)}{\Delta t} \to 0$ as $\Delta t \to 0$. A sensing event leads to an immediate battery energy drop with amount S which is exponentially distributed with mean $E[S]$. Obviously, the battery level $X(t)$ can not be negative. The time of battery outage denoted by $\tau(u, \boldsymbol{\alpha})$ is given by

$$\tau(u, \boldsymbol{\alpha}) = \inf\{t > 0 : X(t) = 0\}, \tag{3.1}$$

and the finite-horizon battery outage probability before the so-called horizon value H denoted by $\psi(u, \boldsymbol{\alpha}, H)$ is then given by

$$\psi(u, \boldsymbol{\alpha}, H) = \Pr\{\tau(u, \boldsymbol{\alpha}) \leq H\}. \tag{3.2}$$

The average sensing rate (denoted by λ_{avg}) represents the average number of transmitted packets i) in the time interval $[0, H]$ if no outage occurs within H, or ii) in the interval $[0, \tau(u, \boldsymbol{\alpha})]$ in case $\tau(u, \boldsymbol{\alpha}) < H$.

3.2 MRMFQ Model

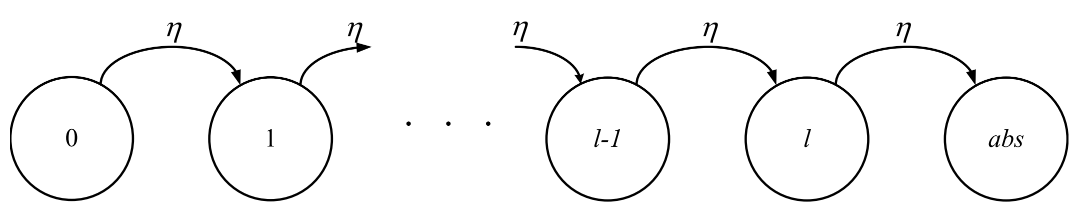

Figure 3.1: l-level Erlangization of the horizon H.

Erlangization refers to approximating a deterministic quantity by an Erlang distribution of sufficiently high order for analytical tractability; see for example [50] that employs Erlangization to approximate the deterministic time horizon in the risk theory context. In this thesis, we employ l-stage Erlangization to model the deterministic horizon H as depicted in Figure 3.1 for various values of the parameter l. The state labeled as *abs* refers to the absorbing state representing the horizon expiration and $\eta = l/H$ is the transition rate from one Erlang stage to the next one. Starting operation at the first stage at time zero, the time to reach the *abs* stage is then Erlang-l distributed with mean H. Clearly, as $l \to \infty$, the Erlang-l distribution converges to a Dirac delta function located at H. We define the following Erlang-l sub-generator T_H and the vector T_H^0 to be used in the MRMFQ model we propose:

$$T_H = \begin{bmatrix} -\eta & \eta & & & \\ & -\eta & \eta & & \\ & & \ddots & \ddots & \\ & & & -\eta & \eta \\ & & & & -\eta \end{bmatrix}, T_H^0 = -T_H \mathbf{1}.$$

The state-space of our MRMFQ model is now described. First, we need l replicas of each harvester state, which are represented by the pair (i, j) for $0 \le i \le N-1$ and $1 \le j \le l$, resulting in a total number of Nl so-called *idle states*, since there is no data transmission in these states. As packets being transmitted, there should be a reduction in the battery level. For this purpose, we need a transmission-mode replica of the idle state (i, j) denoted by $(i, j)^*$ and these Nl replicas will be referred as the *transmitting states*. We introduce three auxiliary states, namely *Outage (O)*, *Reset (R)*, and *Good (G)* states, in order to calculate $\psi(u, \boldsymbol{\alpha}, H)$. Note that within H, either of the two events would occur:

- *No battery outage*: For this event, time expires before the horizon without the battery level hitting zero. We introduce the G and R states to describe the behavior of the battery level in this case. As the horizon expires, the battery level is decreased down to zero (during the G state) and then increased up to the initial level u (in the R state); see Figure 3.2(a).
- *Battery outage*: The battery level hits zero before the horizon. In this case, O state is used to initialize the battery level by increasing it up to u after the battery hits zero; see Figure 3.2(b).

In either case, with the battery level set to u, the system transits into one of the

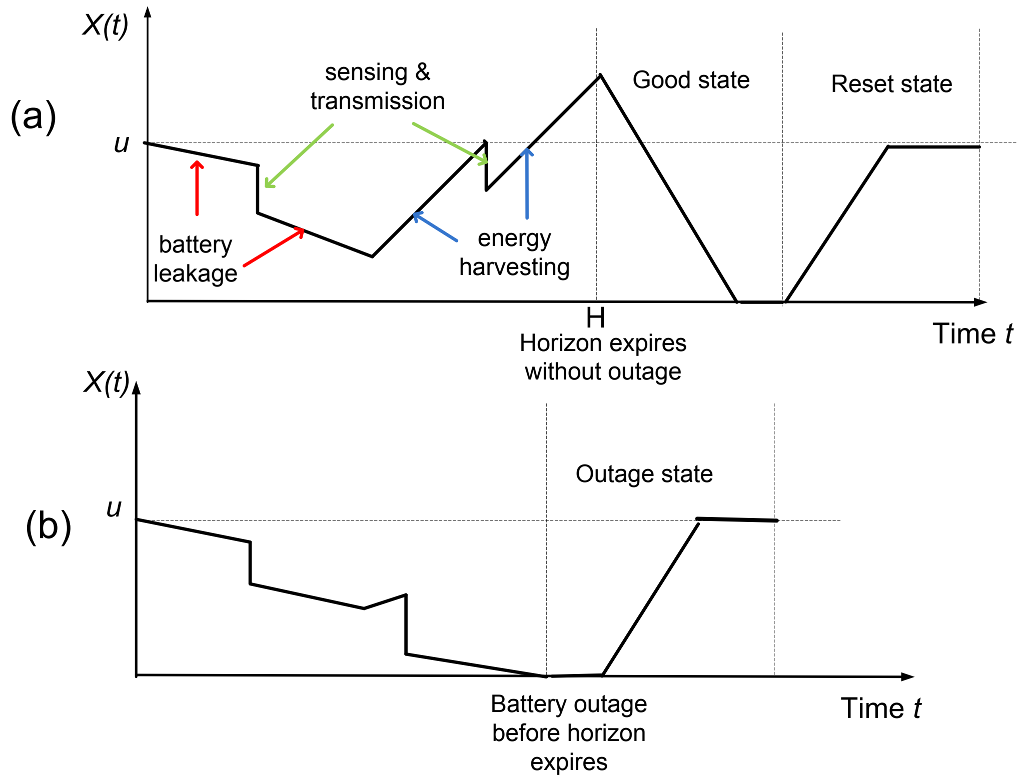

Figure 3.2: Sample paths for (a) no outage, and (b) outage case.

first Erlang states $(i, 1)$, $0 \leq i \leq N-1$ according to the initial probability vector $\boldsymbol{\alpha}$ and the cycle starts over. These two cases are illustrated in Figure 3.2. In this figure, abrupt falls of the battery level represent data transmission and battery leakage (energy harvesting) is shown by a negative (positive) slope.

In our MRMFQ formulation and for numerical accuracy purposes, the energy level is reduced at a finite rate of p_T as opposed to abrupt drops. For this purpose, we choose scalar parameters p_T and β such that the mean dissipated energy for one packet transmission $E[S]$ equals the product p_T/β. Consequently, each time a packet gets to be transmitted, the battery level is allowed to reduce at a rate of p_T for an exponentially distributed amount of time with parameter β leading to an exponentially distributed eventual energy drop with mean $E[S]$. However, this model does not lead to any inaccuracy as will be shown in the sequel. Next, we order the states as (i) O state, (ii) R state, (iii) G state, (iv)

Nl idle states enumerated lexicographically, (v) Nl transmission states enumerated lexicographically. With this state space, we are now ready to describe the MRMFQ model which is a translation of the sample paths provided in Figure 3.2 into an MRMFQ that uses the regime boundaries $T^{(k)}, 0 \le k \le K$. Therefore, in the proposed MRMFQ model, the regime-k generator matrix is written as

$$Q^{(k)} = \begin{bmatrix} 0 & 0 & 0 & \mathbf{0} & \mathbf{0} \\ 0 & 0 & 0 & \mathbf{0} & \mathbf{0} \\ 0 & 0 & 0 & \mathbf{0} & \mathbf{0} \\ \mathbf{0} & \mathbf{0} & \mathbf{1} \otimes T_H^0 & \mathbf{I} \otimes T_H + (Q - \Lambda(k)) \otimes \mathbf{I} & \Lambda(k) \otimes \mathbf{I} \\ \mathbf{0} & \mathbf{0} & \mathbf{0} & \beta \mathbf{I} & -\beta \mathbf{I} \end{bmatrix}. \tag{3.3}$$

The boundary-k generator matrix $\tilde{Q}^{(k)} = Q^{(k)}$ for $k \in \{1, 2, \dots, J-1, J+1, \dots, K\}$. However, the boundary-0 and boundary-J generators require more work. In particular

$$\tilde{Q}^{(J)} = \begin{bmatrix} -1 & 0 & 0 & \boldsymbol{\alpha} \otimes \boldsymbol{e}_1 & \mathbf{0} \\ 0 & -1 & 0 & \boldsymbol{\alpha} \otimes \boldsymbol{e}_1 & \mathbf{0} \\ 0 & 0 & 0 & \mathbf{0} & \mathbf{0} \\ \mathbf{0} & \mathbf{0} & \mathbf{1} \otimes T_H^0 & \mathbf{I} \otimes T_H + (Q - \Lambda(J)) \otimes \mathbf{I} & \Lambda(J) \otimes \mathbf{I} \\ \mathbf{0} & \mathbf{0} & \mathbf{0} & \beta \mathbf{I} & -\beta \mathbf{I} \end{bmatrix} \tag{3.4}$$

and

$$\tilde{Q}^{(0)} = \begin{bmatrix} 0 & 0 & 0 & \mathbf{0} & \mathbf{0} \\ 0 & 0 & 0 & \mathbf{0} & \mathbf{0} \\ 0 & 1 & -1 & \mathbf{0} & \mathbf{0} \\ \mathbf{1} & \mathbf{0} & \mathbf{0} & -\mathbf{I} & \mathbf{0} \\ \mathbf{1} & \mathbf{0} & \mathbf{0} & \mathbf{0} & -\mathbf{I} \end{bmatrix}. \tag{3.5}$$

The regime-k and boundary-k drift matrices of the proposed MRMFQ are given as follows:

$$R^{(k)} = \begin{cases} \mathbf{diag}(1, 1, -1, D \otimes \mathbf{I}, -p_T\mathbf{I}), & 1 \leq k \leq J, \\ \mathbf{diag}(-1, -1, -1, D \otimes \mathbf{I}, -p_T\mathbf{I}), & J < k \leq K. \end{cases} \tag{3.6}$$

$$\tilde{R}^{(k)} = \begin{cases} R^{(k)}, & k \notin \{0, J, K\}, \\ \mathbf{max}(0, R^{(1)}), & k = 0, \\ \mathbf{diag}(0, 0, -1, D \otimes \mathbf{I}, -p_T\mathbf{I}), & k = J, \\ \mathbf{min}(0, R^{(K)}), & k = K, \end{cases} \tag{3.7}$$

where the **max** and **min** are element-wise operators. Under this choice, note that the amount of time spent in the O and R states during each visit to these two states possess the same distribution. This observation holds also for the time spent in these two states restricted to $x = u$. Therefore, the finite-horizon battery outage probability $\psi(u, \boldsymbol{\alpha}, H)$ can be written as

$$\psi(u, \boldsymbol{\alpha}, H) = \frac{c_O^{(J)}}{c_O^{(J)} + c_R^{(J)}}, \tag{3.8}$$

where $c_R^{(J)}$ and $c_O^{(J)}$[1] as the probability mass accumulations of the proposed MRMFQ at the boundary J in states R and O, respectively.

3.3 Engineering Framework

By solving the mathematical model described above, we now derive an expression to calculate the average sensing rate λ_{avg}. Subsequently, we study various adaptive sensing rate policies to maximize the average sensing rate where the system requirement is the finite-horizon outage probability given in (3.8) being less than a given desired probability ψ_T. According to the battery level, the sensing rate

[1] Note that since $c_R^{(J)} = c_G^{(0)}$ where $c_G^{(0)}$ is the probability mass accumulation at the boundary 0 in state G, $c_R^{(J)}$ and $c_G^{(0)}$ can be used in Eqn. (3.8) interchangeably.

$\lambda_i(k)$ is allowed to take either a minimum or a maximum value, denoted by λ_{min} and λ_{max}, respectively. The optimization problem we deal with can be written as:

$$\begin{aligned} \underset{\lambda_i(k)}{\text{maximize}} \quad & \lambda_{avg} \\ \text{subject to} \quad & \psi(u, \boldsymbol{\alpha}, H) < \psi_T, \\ & \lambda_i(k) = \lambda_{min}, \lambda_{max} \end{aligned} \tag{3.9}$$

for $1 \leq k \leq K$. Intuitively, when the battery level is close to zero, the rate should be set to λ_{min} to avoid battery outage. Similarly, the SN should sense the environment with rate λ_{max} when the battery is almost fully charged to provide enough space in the battery for new energy arrivals. This leads us to investigate a threshold-based structure for $\lambda_i(k)$. In this thesis, we assume a two-state EHP with two harvester states 0 and 1 and the thresholds for these states are denoted by B_0 and B_1, respectively. The value of $\lambda_i(k)$ in each regime can be written as follows:

$$\lambda_i(k) = \begin{cases} \lambda_{min}, & X(t) \leq B_i, \\ \lambda_{max}, & X(t) > B_i. \end{cases}$$

Since we let each state have its own threshold, we refer to this policy as the State-Dependent Threshold Policy (SDTP). SDTP being employed for a two-state energy harvesting process results in a 4-regime MFQ. Together with the boundary points at $T^{(0)} = 0$, $T^{(J)} = u$ and $T^{(K)} = T^{(4)} = B$, we have two more boundary points each of which corresponds to the threshold of one harvester state. For instance, if $B_1 < u < B_0$, we have $T^{(1)} = B_1$, $T^{(2)} = u$ and $T^{(3)} = B_0$. Similarly, if $B_1 < B_0 < u$, the boundary points can be written as $T^{(1)} = B_1$, $T^{(2)} = B_0$ and $T^{(3)} = u$, and so on. As an example, the SDTP policy for the case $B_1 < u < B_0 < B$ is illustrated in Figure 3.3. Note that two or more boundary points may coincide, which will not have any adverse effect on the solution methodology. Similar to the power-save mode proposed in [52], we also define the Single Threshold Policy (STP) for which there is a single threshold for the battery level regardless of the harvester state, i.e., $B_0 = B_1$. Clearly, STP can be modeled with a 3-regime MRMFQ.

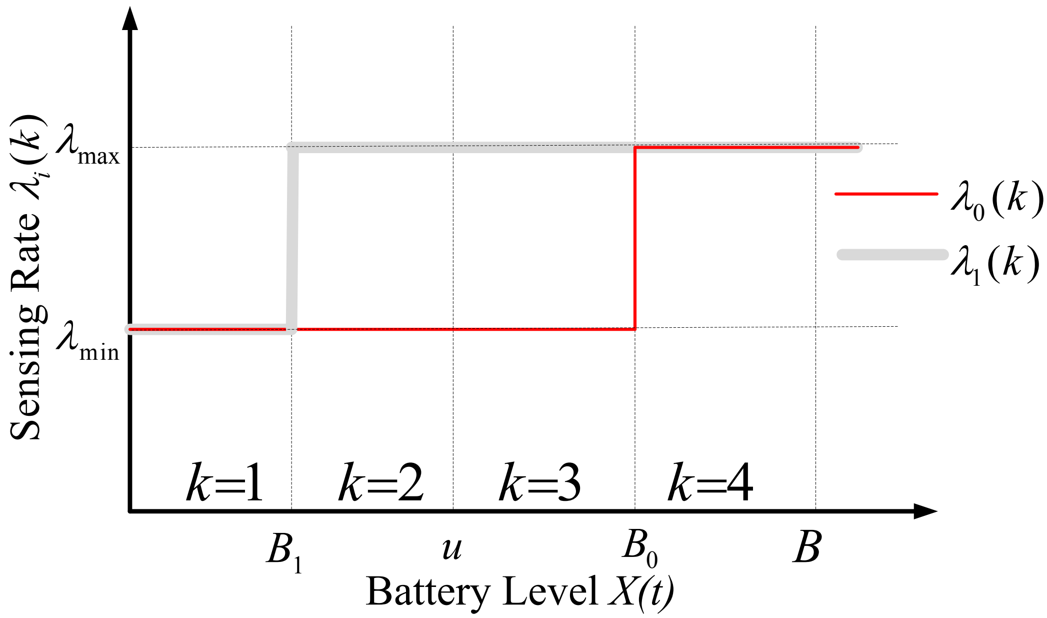

Figure 3.3: Sensing rate $\lambda_i(k)$ of SDTP for the case $B_1 < u < B_0 < B$.

We denote the steady-state joint pdf and probability mass accumulations of idle state (i, m) in regime k by $f_{(i,m)}^{(k)}(x)$ and $c_{(i,m)}^{(k)}$, respectively. To calculate the average sensing rate λ_{avg}, we also denote the normalized steady-state joint pdf and probability mass accumulations $\hat{f}_{(i,m)}^{(k)}(x)$ and $\hat{c}_{(i,m)}^{(k)}$ for idle states. Since O, R, and G are auxiliary states which are defined to calculate the outage probability, we censor out these states in the calculation of the average sensing rate. Transmitting states also need to be censored out since transmissions are modeled as abrupt falls of the instantaneous battery level. Finally, since probability mass accumulations at zero occur due to battery outage, we also censor them out. Subsequently, we write the normalized the steady-state joint pdf $\hat{f}_{(i,m)}^{(k)}(x)$ as

$$\hat{f}_{(i,m)}^{(k)}(x) = \frac{f_{(i,m)}^{(k)}(x)}{\sum\limits_{i=0}^{N-1} \sum\limits_{m=1}^{l} \sum\limits_{k=1}^{K} \left(\int\limits_{T^{(k-1)}+}^{T^{(k)}-} f_{(i,m)}^{(k)}(x)dx + \sum\limits_{k=1}^{K} c_{(i,m)}^{(k)} \right)}. \tag{3.10}$$

The quantities $\hat{c}_{(i,m)}^{(k)}$ can be obtained similarly. With these normalized quantities, one can calculate the average sensing rate as follows:

$$
\begin{aligned}
\lambda_{avg} &= \sum_{i=0}^{N-1} \lambda_{min} \Pr\{Z(t)=i, X(t) \leq B_i\} + \lambda_{max} \Pr\{Z(t)=i, X(t) > B_i\} \\
&= \sum_{i=0}^{N-1} \sum_{m=1}^{l} \left[\lambda_{min} \sum_{k=1}^{\overline{K_i}} \left(\int_{T^{(k-1)}+}^{T^{(k)}-} \hat{f}_{(i,m)}^{(k)}(x)dx + \hat{c}_{(i,m)}^{(k)} \right) \right] \\
&+ \sum_{i=0}^{N-1} \sum_{m=1}^{l} \left[\lambda_{max} \sum_{k=\underline{K_i}}^{K} \left(\int_{T^{(k-1)}+}^{T^{(k)}-} \hat{f}_{(i,m)}^{(k)}(x)dx + \hat{c}_{(i,m)}^{(k)} \right) \right] \qquad (3.11)
\end{aligned}
$$

where $\overline{K_i}$ ($\underline{K_i}$) is the value of k such that $T^{(k)} = B_i$ ($T^{(k-1)} = B_i$). With the expressions derived for the battery outage probability and average sensing rate in terms of the steady-state solution of a certain MRMFQ with $2Nl+3$ states, one can solve for the outage probabilities as a function of the pair (B_0, B_1). The particular values of this pair that yield the largest average sensing rate among those that yield $\psi(u, \boldsymbol{\alpha}, H) < \psi_T$ are to be chosen as the optimal pair of threshold parameters. A numerical example that describes the step-by-step solution procedure for a two-state CTMC is given in the Appendix.

Chapter 4

Numerical Examples

In this section, we first validate the accuracy of the proposed analytical method by comparing the analytical results with the ones obtained by the simulations. Then, we examine threshold-based policies and evaluate the performance of a so-called State Dependent Threshold Policy (SDTP) by comparing it with two other policies for an exhaustive set of parameters.

4.1 Model Parameters

In this section, we identify the system parameters including the parameters of the rechargeable battery, transmission scenario and energy harvester model.

4.1.1 Rechargeable Battery Model

As candidate power supplies for energy harvesting SNs, properties of five different rechargeable battery technologies, namely Sealed Lead Acid (SLA), Nickel Cadmium (NiCd), Nickel Metal Hydride (NiMH), Lithium Ion (Li-ion) and Lithium Polymer (Li-polymer) are investigated in [18]. Two of the most commonly used rechargeable battery types are Li-based and NiMH. Li-based batteries outperform NiMH batteries in several axes such as higher energy-power densities and charging efficiency and lower self-discharge rate. However, recharging Li-based batteries requires considerably complicated charging circuits. On the other hand, NiMH batteries do not require any charging circuits while achieving reasonable performance in terms of the aforementioned parameters. Hence, we propose in this thesis to use NiMH batteries as the power supply of an SN. Important properties of this particular type of battery which are used in the numerical analysis are tabulated in Table 4.1 [18]. The last column of Table 4.1 shows the *self discharge rate* of the battery, which is the percentage loss of the battery per month without any connections. In the numerical examples, the unit of time is taken to be hours. 30 %/month self-discharge rate results in 1.25 mWh lost energy in one hour for a 3000 mWh battery. We use a constant-power battery leakage model by fixing $l_b = 1.25$ mW.

Table 4.1: Properties of NiMH batteries.

Nominal Voltage (V)	Capacity (mAh)	Capacity (mWh)	Charging Efficiency (%)	Self Discharge (%/month)
1.2	2500	3000	66	30

4.1.2 Transmission Model

We use the first order radio model given in [62], with assuming a d^4 energy loss as a function of distance d. According to this model, SN consumes:

$$E_{Tx}(k,d) = E_{elec}k + \epsilon_{amp}kd^4 \tag{4.1}$$

of energy to transmit a k-bit packet over a distance d. E_{elec} and ϵ_{amp} are the amounts of energy that the transmitter circuitry and amplifier consume per bit, respectively. In the examples, we set $E_{elec} = 50$ nJ/bit, $\epsilon_{amp} = 100$ pJ/bit/m^4, $d = 100$ m and assume exponentially distributed packet sizes with mean 1000 bytes. We also assume a bit rate of 1 Mbps. This means SN expends $k(E_{elec} + \epsilon_{amp}d^4) = k(5 \cdot 10^{-8} + 10^{-2}) \approx k \cdot 10^{-2}$ J to transmit one bit. Considering the mean packet size of 1000 bytes, it requires $E[S] = 80$ J ≈ 22.222 mWh to transmit one packet on average. Accordingly, we set $p_T = 10$ and $\beta = 0.45$, which results in $E[S] = p_T/\beta = 22.222$.

4.1.3 Energy Harvester Model

The sensor node considered in the numerical examples is equipped with a solar cell of size 37×33 mm^2. First, we assume a two-state ("on" and "off") CTMC as the EHP. As discussed in [18], for 100 mW/cm^2 of available power, solar cells can provide an output power of 15 mW/cm^2 with 15% conversion efficiency. Considering a constant output power of 15 mW/cm^2 for a 37×33 mm^2 solar cell, approximately 183 mWh of energy can be obtained in one hour. Since the charging efficiency of the NiMH battery is 66%, 120 mWh of this energy can be stored in the battery. In order to use a realistic EHP model which also complies with the real world data, several studies have been investigated including [37] and [44]. In [37], two types of quantizers, coarse (two-state) and fine (twenty-state), are experimented to fit a first-order Markovian model to empirically measured data. For simplicity, we choose a two-state background process to model the harvested energy. The authors in [44] use a similar two-state process and report simulations results for 4 combinations of transition rates for on and off states as (ordered as on-off) 1-1, 1-12, 12-1 and 12-12 hour^{-1}, in order to obtain results for both fast and slow switching between the states. Moreover, annual data records of the solar irradiance measured in Washington, Oregon, Idaho, Montana and Wyoming reveal that the average solar radiation is approximately 4 kWh/m^2, which is equal to 4884 mWh of available energy per day [63]. Since we assume a conversion efficiency of 15%, this results in approximately 732 mWh of daily harvested energy. By taking all this information into account, we consider the following energy harvesting model: Solar cell outputs either 120 mW (h_1) or 0 mW (h_2) for exponentially distributed time intervals with means 1 and 5 hours, respectively, according to the state of the EHP. This means on average, $20 \times 0 + 4 \times 120 = 480$ mWh (727 mWh) energy is stored (harvested) daily at 66% charging efficiency, which complies with the measurements in [63].

4.2 Example I - Validation

In the first example, we verify the accuracy of the outage probability and average sensing rate expressions derived in Chapter 3. For this purpose, the system is simulated for 10^5 time cycles where a time cycle refers to a single horizon for each of which we keep track of whether outage has occurred or not, and additionally the number of overall transmitted packets. As the system parameters, we set $H = 1$, $\lambda_{max} = 4$, $B_1 = 1500$, and $B_0 = 2500$, and vary λ_{min} from 0.4 to 1.3 and compare the resulting outage probabilities and average sensing rates with the simulation results in Figures 4.1, 4.2 and 4.3 for $u = 750, 2000, 2750$, respectively. For all of the following examples, we set $\boldsymbol{\alpha} = \begin{bmatrix} 5/6 & 1/6 \end{bmatrix}$ unless otherwise stated.

We observe that as the number of Erlangization levels l increases, analytical results of $\psi(u, \boldsymbol{\alpha}, H)$ converge to the simulation results, while the average sensing rate seems to be less sensitive to l. A notable accuracy is obtained with the choice of $l = 50$ (requires a computation time of approximately 0.6 seconds for one problem instance with MATLAB running on a notebook using an Intel Core i5-3210M Processor and a RAM of 8 GB) for both performance metrics. Therefore, we set l to 50 for the remaining examples.

The outage probability is depicted as a function of B_1 for B_0 being fixed to 1500 and $H = 1, 3, 12$ in Figure 4.4. Other parameters are set to $u = 3000$, $\lambda_{min} = 0.4$, $\lambda_{max} = 10$. In all the cases shown in Figure 4.4, the findings of the analytical method overlap with the simulation results. We also compare the analytical results with simulations for various values of the initial probability vector $\boldsymbol{\alpha}$ and $u = 100, 200, 300, 400, 500$. We set $\lambda_{min} = 0.5$, $\lambda_{max} = 4$, $H = 1$, $B_0 = 2000$, $B_1 = 1000$, $\boldsymbol{\alpha} = [(1 - \alpha_1)\ \alpha_1]$ and vary α_1 from 0 to 1. As illustrated in Figure 4.5, the initial harvester state is more important for relatively lower values of the initial battery level u. Again, we observe that the analytical results are in line with simulations.

For validation purposes, we also investigate the case in which a moderate sensing rate, denoted by λ_{mod}, is introduced which results in two thresholds for

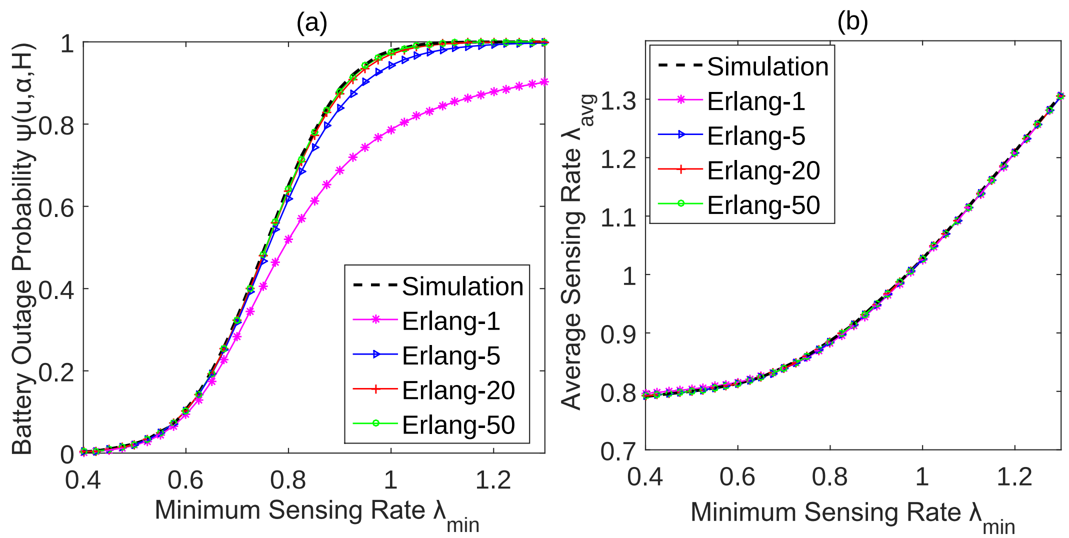

Figure 4.1: (a) Battery outage probability $\psi(u, \boldsymbol{\alpha}, H)$ and (b) average sensing rate λ_{avg}, as functions of λ_{min} for $H = 1$, $\lambda_{max} = 4$, $B_1 = 1500$, $B_0 = 2500$ and $u = 750$.

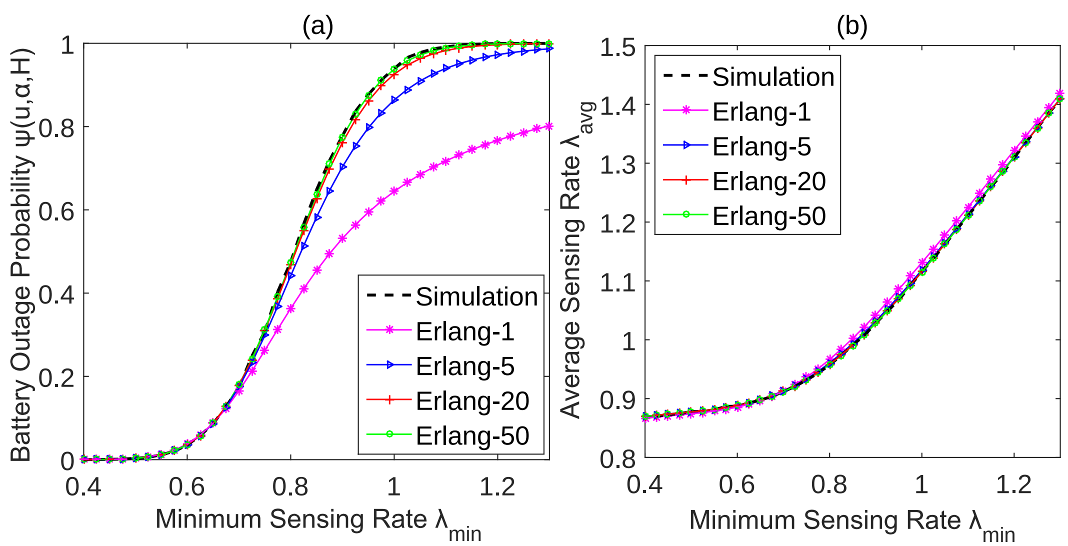

Figure 4.2: (a) Battery outage probability $\psi(u, \boldsymbol{\alpha}, H)$ and (b) average sensing rate λ_{avg}, as functions of λ_{min} for $H = 1$, $\lambda_{max} = 4$, $B_1 = 1500$, $B_0 = 2500$ and $u = 2000$.

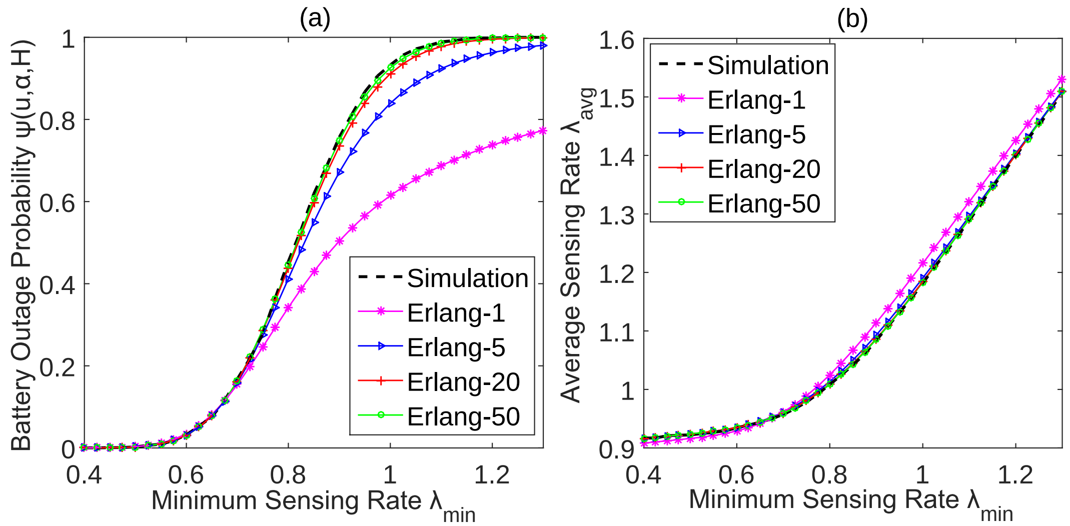

Figure 4.3: (a) Battery outage probability $\psi(u, \boldsymbol{\alpha}, H)$ and (b) average sensing rate λ_{avg}, as functions of λ_{min} for $H = 1$, $\lambda_{max} = 4$, $B_1 = 1500$, $B_0 = 2500$ and $u = 2750$.

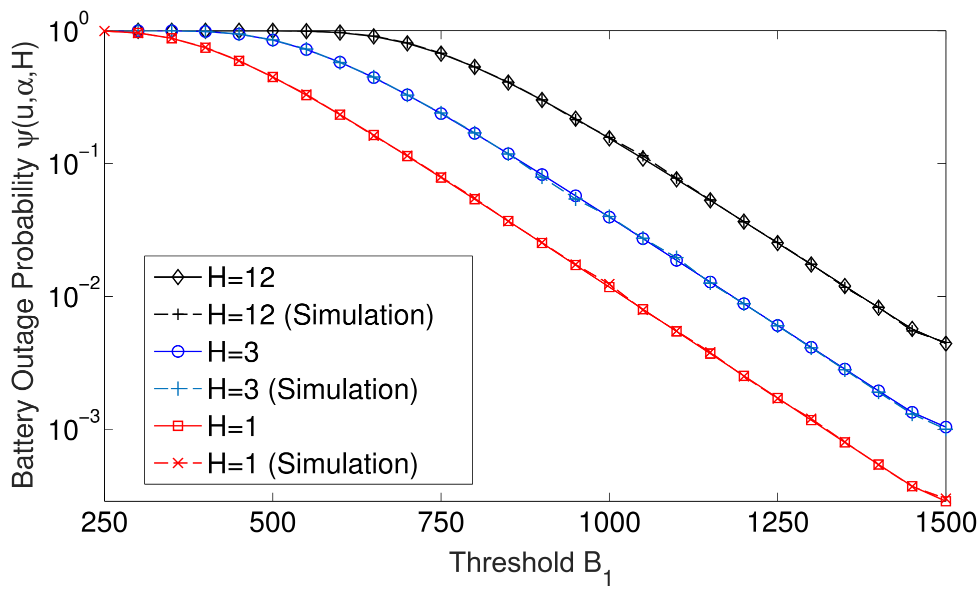

Figure 4.4: Battery outage probability as a function of B_1 for $H = 1, 3, 12$ and $u = 3000$, $\lambda_{min} = 0.4$, $\lambda_{max} = 10$, $\boldsymbol{\alpha} = [5/6\ 1/6]$.

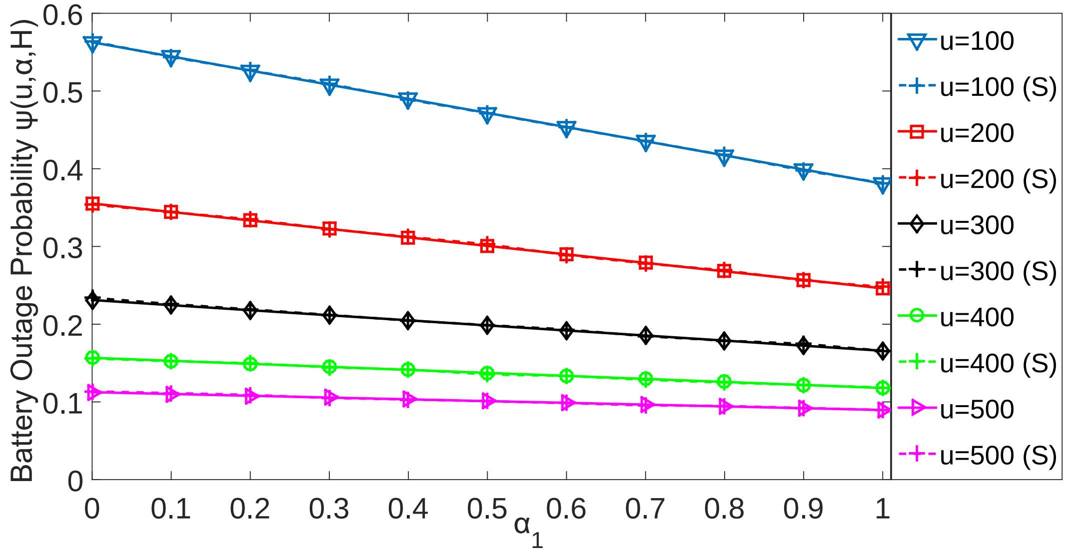

Figure 4.5: Battery outage probability as a function of $\boldsymbol{\alpha} = [(1-\alpha_1)\ \alpha_1]$ for $u = 100, 200, 300, 400, 500$ and $\lambda_{min} = 0.5$, $\lambda_{max} = 4$, $H = 1$, $B_0 = 2000$, $B_1 = 1000$.

each state and four thresholds in total. We denote the thresholds of state i by $B_{i,1}$ and $B_{i,2}$ for $i = 1, 2$ such that the sensing rate $\lambda_i(k)$ is given by the following expressions:

$$\lambda_i(k) = \begin{cases} \lambda_{min}, & X(t) \leq B_{i,1}, \\ \lambda_{mod}, & B_{i,1} < X(t) \leq B_{i,2}, \\ \lambda_{max}, & X(t) > B_{i,2}. \end{cases}$$

As the other system parameters, we set $\lambda_{min} = 0.4$, $\lambda_{max} = 2$, $\lambda_{max} = 10$, $B_{0,1} = 1500$, $B_{0,2} = 2250$, $B_{1,1} = 500$, $B_{1,2} = 1250$, $u = B = 3000$, $\boldsymbol{\alpha} = [5/6\ 1/6]$ and tabulate the analytical and simulation results for the finite-horizon battery outage probability $\psi(u, \boldsymbol{\alpha}, H)$ and average sensing rate λ_{avg} for $H = 1, 3, 6, 9, 12$ in Table 4.2. We also provide 98% confidence intervals for $\psi(u, \boldsymbol{\alpha}, H)$ in the simulations results. We observe that the simulation and analytical results comply with each other also for a four-threshold model. These results reveal that the analytical method is capable of analyzing similar multi-threshold systems and its extension to cases in which there are more numbers of possible sensing rates is straightforward.

Table 4.2: Comparison of analytical and simulation results for $\lambda_{min} = 0.4$, $\lambda_{mod} = 2$, $\lambda_{max} = 10$, $B_{0,1} = 1500$, $B_{0,2} = 2250$, $B_{1,1} = 500$, $B_{1,2} = 1250$, $u = B = 3000$, $\boldsymbol{\alpha} = [5/6\ 1/6]$ and $H = 1, 3, 6, 9, 12$.

H	$\psi(u, \boldsymbol{\alpha}, H)$			λ_{avg}	
	Analytical Result	Simulation Result	Simulation 98% Conf. Int.	Analytical Result	Simulation Result
1	0.0135	0.0134	± 0.0007	0.9677	0.9677
3	0.0499	0.0503	± 0.0014	0.8867	0.8869
6	0.1019	0.1021	± 0.0019	0.8664	0.8665
9	0.1510	0.1514	± 0.0022	0.8597	0.8597
12	0.1974	0.1977	± 0.0025	0.8563	0.8565

4.3 Example II - Fixed Sensing Rate Policy (FSRP)

Let us now assume a Fixed Sensing Rate Policy (FSRP) for which the sensing rate $\lambda(X(t), Z(t))$ does not depend on $X(t)$ or $Z(t)$ and equals λ. For a given desired outage probability ψ_T, we define the maximum attainable fixed sensing rate λ^* called the *limit-sensing rate* which meets the outage probability constraint. In this case, the MRMFQ possesses two regimes with $T^{(0)} = 0 < T^{(1)} = u \leq T^{(2)} = B$. For this example, we assume that the battery is initially fully charged, i.e., $u = B = 3000$, and the horizon H is varied from 1 to 24 months. For other parameters being fixed, one can easily obtain the value of λ^* by binary search. The limit sensing rate λ^* is depicted in Figure 4.6 as a function of the horizon H for four different values of ψ_T, namely 0.01, 0.025, 0.05 and 0.1. We observe that λ^* decreases as H increases. Moreover, as the outage probability constraint is relaxed and ψ_T is increased, higher sensing rates can be achieved while meeting the lifetime constraint. For the threshold-based policies, one should make sure that $\lambda_{min} < \lambda^*$ so that the system is functional and the battery level remains positive throughout the specified horizon for a given ψ_T. Moreover, λ_{max} may be selected as large as the application requires in order to utilize the harvested energy.

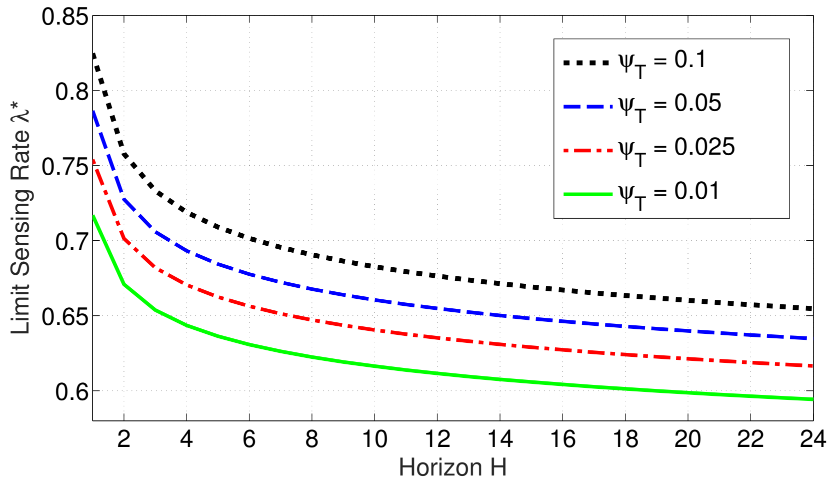

Figure 4.6: The limit sensing rate λ^* as a function of the horizon H for four different values of ψ_T.

4.4 Example III - State-Dependent Threshold Policy (SDTP)

In this example, we set $H = 12$, $\lambda_{min} = 0.4$, $\lambda_{max} = 10$ and $u = 3000$, which means the battery is initially fully charged. We first show how $\psi(u, \boldsymbol{\alpha}, H)$ and λ_{avg} change as thresholds B_0 and B_1 vary between $[0, 3000]$ in Figures 4.7 and 4.8 from which one can obtain the values of B_0 and B_1 that maximize λ_{avg} while satisfying $\psi(u, \boldsymbol{\alpha}, H) < \psi_T$ for a given ψ_T. We denote these particular values by B_0^* and B_1^*. In Figure 4.9, we demonstrate how the optimal thresholds B_0^* and B_1^* behave as a function of H when $\psi_T = 0.1$, along with B^* the optimal threshold for STP. For all values of H, B^* appears to lie between B_0^* and B_1^* but for this example, all optimal thresholds appear to be close. For the same example, the average sensing rates λ_{avg} obtained by SDTP, and STP, and the limit sensing rate λ^* is depicted in Figure 4.10 as a function of the horizon parameter H. We observe that adaptive sensing increases substantially the average sensing rate if the adaptation is performed optimally. Moreover, the average sensing rate obtained by SDTP is slightly better than that of STP.

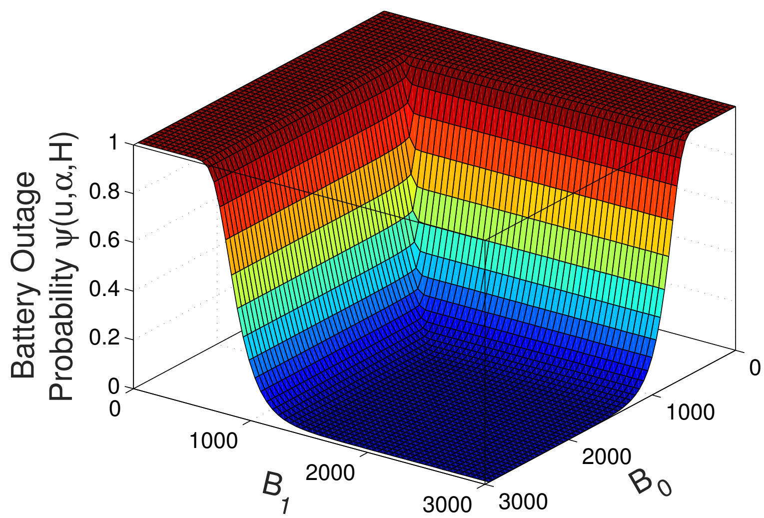

Figure 4.7: Battery outage probability $\psi(u, \boldsymbol{\alpha}, H)$ as a function of B_0 and B_1 for $u = 3000$, $H = 12$, $\lambda_{min} = 0.4$ and $\lambda_{max} = 10$.

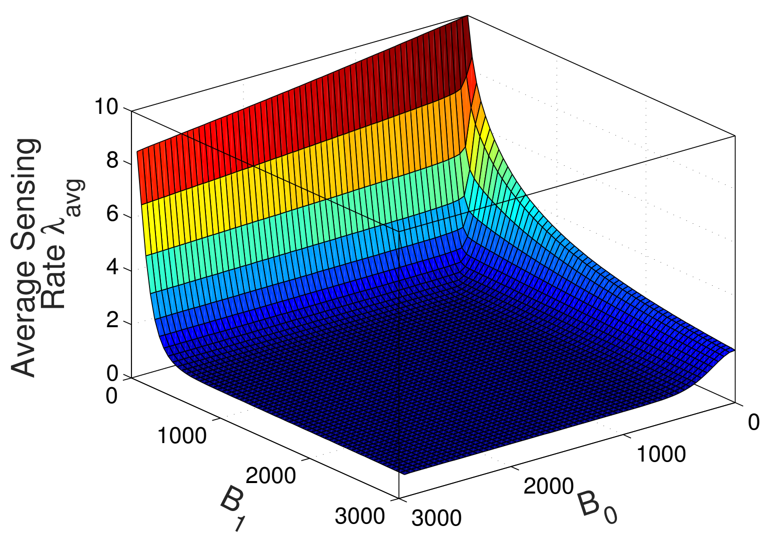

Figure 4.8: Average sensing rate λ_{avg} as a function of B_0 and B_1 for $u = 3000$, $H = 12$, $\lambda_{min} = 0.4$ and $\lambda_{max} = 10$.

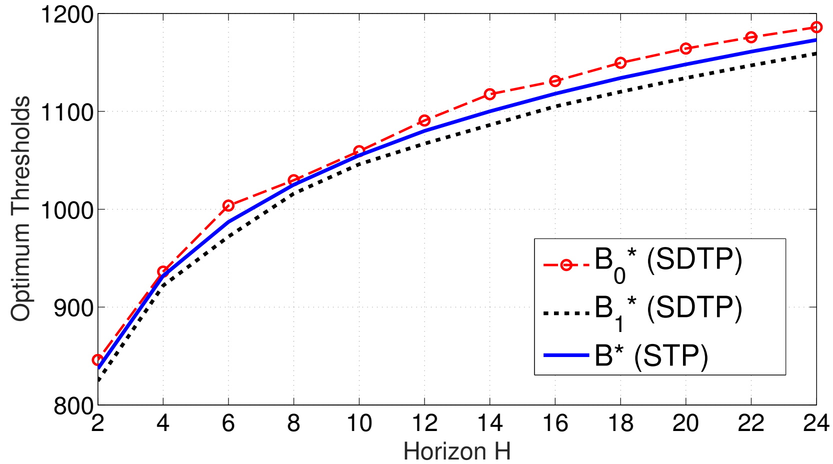

Figure 4.9: optimal thresholds B_0^*, B_1^*, and B^* as functions of the horizon H for $\psi_T = 0.1$, $u = 3000$, $\boldsymbol{\alpha} = [5/6\ 1/6]$, $\lambda_{min} = 0.4$ and $\lambda_{max} = 10$.

We now consider a 100-times slower EHP whose transition rates out of harvester states 1 and 0 are 1/500 and 1/100, respectively. For the following scenario, we set $\boldsymbol{\alpha} = \begin{bmatrix} 1 & 0 \end{bmatrix}$, which means that the initial harvester state is always 0. We also set $\lambda_{min} = 0.9\lambda^*$ for all values of H. The other parameters are the same as in the previous scenario. We again plot the optimal thresholds and average sensing rates in Figures 4.11 and 4.12, respectively. B^* still lies between B_0^* and B_1^* which are quite apart from each other. Moreover, STP is substantially outperformed by SDTP in terms of the average sensing rate. Similar to the relatively faster EHP, both SDTP and STP outperform FSRP for this example as well.

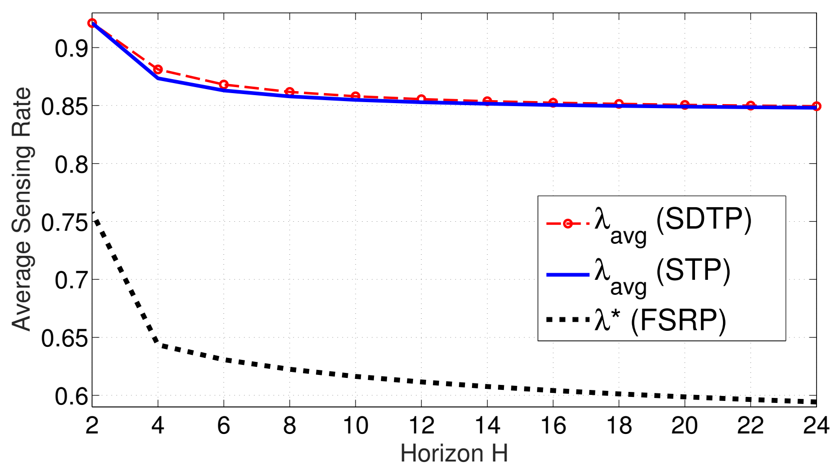

Figure 4.10: Average sensing rates λ_{avg} and limit sensing rate λ^* as functions of the horizon H for $\psi_T = 0.1$, $u = 3000$, $\boldsymbol{\alpha} = [5/6\ 1/6]$, $\lambda_{min} = 0.4$ and $\lambda_{max} = 10$.

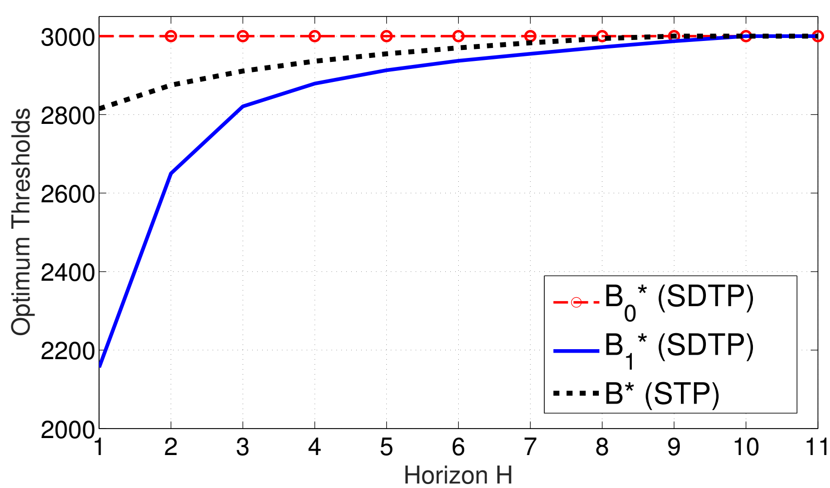

Figure 4.11: optimal thresholds B_0^*, B_1^*, and B^* for 100-times slower process as functions of the horizon H for $\psi_T =, 0.1$, $u = 3000$, $\boldsymbol{\alpha} = [1\ \ 0]$, $\lambda_{min} = 0.9\lambda^*$ and $\lambda_{max} = 10$.

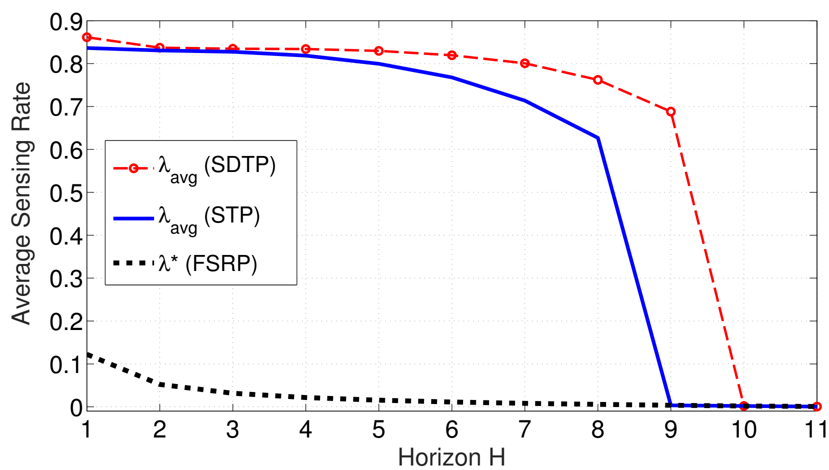

Figure 4.12: Average sensing rates λ_{avg} and limit sensing rate λ^* for 100-times slower process as functions of the horizon H for $\psi_T = 0.1$, $u = 3000$, $\boldsymbol{\alpha} = [1 \ \ 0]$, $\lambda_{min} = 0.9\lambda^*$ and $\lambda_{max} = 10$.

Chapter 5

Conclusions

We propose in this thesis a risk-theoretic multi-regime Markov fluid queue-based method for computing the finite-horizon battery outage probabilities in energy harvesting sensor nodes with energy management. For energy management, we focus on threshold-based energy management policies in which a high (low) sensing rate is applied when the battery level is above (below) a certain threshold. We propose to use Erlangization to cope with the deterministic finite time horizon. We validate the accuracy of the proposed method by comparing the results with simulations for an exhaustive set of system parameters. We show that as the Erlangization level of the horizon increases, the analytical results converge to those obtained by simulations. Considering the computational inefficiency of simulations which requires hours to execute (or even days for large horizon values), the validation section put emphasis the computational efficiency of the proposed method. Subsequently, we use this method as the engine of an optimization framework by which we determine the optimal operational parameters of a so-called State-Dependent Threshold Policy (SDTP) which maximizes the average sensing rate while satisfying finite-horizon battery outage probability constraints and for which there is a separate threshold for each state of the underlying EHP. As shown in the final example, threshold-based policies significantly increase the average sensing rate for a given lifetime constraint compared to the benchmark policy Fixed Sensing Rate Policy (FSRP); whereas selecting state-dependent thresholds may further enhance the system performance, depending on the energy harvesting scenario. For relatively faster EHPs, which is more common in energy harvesting environments, Single Threshold Policy (STP) may be preferred over SDTP as the energy management policy since it employs a single threshold for all the states of the EHP which is simpler and faster to compute.

Extensions of this work will consist of more sophisticated models where sensing and packet transmission may be uncoupled leading to two queues; one queue for energy and the other for data. Another future work will be related to obtaining optimal sensing rate policies more general than the double-valued policies (λ_{min} or λ_{max}) studied in this work. Although we focus on the case where one threshold is employed for each state and analyze it comprehensively, we validate that the proposed methodology also works for multiple threshold scenarios which makes it a useful tool to analyze other threshold-based sensing policies.

For simplicity of the demonstration of the proposed method, the energy dissipated for one data packet is assumed to be exponentially distributed in this thesis. However, future work will cover more other statistical distributions such as PH (Phase Type) since the proposed solution framework is extensible for more general distributions.

Bibliography

[1] K. Ashton, "That 'Internet of Things' thing," *RFID Journal*, 2009.

[2] J. Gubbi, R. Buyya, S. Marusic, and M. Palaniswami, "Internet of Things (IoT): A vision, architectural elements, and future directions," *Future Generation Computer Systems*, vol. 29, no. 7, pp. 1645 – 1660, 2013.

[3] "Internet of Things: Wireless sensor networks," tech. rep., International Electrotechnical Commission (IEC), 2014.

[4] P. Kamalinejad, C. Mahapatra, Z. Sheng, S. Mirabbasi, V. C. M. Leung, and Y. L. Guan, "Wireless energy harvesting for the internet of things," *IEEE Communications Magazine*, vol. 53, pp. 102–108, June 2015.

[5] "Energy harvesting wireless power for the Internet of Things," tech. rep., EnOcean, 2015.

[6] M. T. Lazarescu, "Design of a WSN platform for long-term environmental monitoring for iot applications," *IEEE Journal on Emerging and Selected Topics in Circuits and Systems*, vol. 3, pp. 45–54, March 2013.

[7] "The evolution of wireless sensor networks," tech. rep., Silicon Labs, 2013.

[8] I. Akyildiz, W. Su, Y. Sankarasubramaniam, and E. Cayirci, "A survey on sensor networks," *Communications Magazine, IEEE*, vol. 40, pp. 102–114, Aug 2002.

[9] J. Yick, B. Mukherjee, and D. Ghosal, "Wireless sensor network survey," *Computer Networks*, vol. 52, no. 12, pp. 2292 – 2330, 2008.

[10] T. Arampatzis, J. Lygeros, and S. Manesis, "A survey of applications of wireless sensors and wireless sensor networks," in *Intelligent Control, 2005. Proceedings of the 2005 IEEE International Symposium on, Mediterrean Conference on Control and Automation*, pp. 719–724, June 2005.

[11] Q. Zhu, R. Wang, Q. Chen, Y. Liu, and W. Qin, "IOT gateway: Bridgingwireless sensor networks into Internet of Things," in *Embedded and Ubiquitous Computing (EUC), 2010 IEEE/IFIP 8th International Conference on*, pp. 347–352, Dec 2010.

[12] S. Soro and W. Heinzelman, "Prolonging the lifetime of wireless sensor networks via unequal clustering," in *Parallel and Distributed Processing Symposium, 2005. Proceedings. 19th IEEE International*, pp. 236–244, April 2005.

[13] Y. Chen and Q. Zhao, "On the lifetime of wireless sensor networks," *Communications Letters, IEEE*, vol. 9, pp. 976–978, Nov 2005.

[14] A. Mainwaring, D. Culler, J. Polastre, R. Szewczyk, and J. Anderson, "Wireless sensor networks for habitat monitoring," in *Proceedings of the 1st ACM International Workshop on Wireless Sensor Networks and Applications*, WSNA '02, (New York, NY, USA), pp. 88–97, ACM, 2002.

[15] M. Cardei and D.-Z. Du, "Improving wireless sensor network lifetime through power aware organization," *Wirel. Netw.*, vol. 11, pp. 333–340, May 2005.

[16] W. Ye, J. Heidemann, and D. Estrin, "An energy-efficient MAC protocol for wireless sensor networks," in *INFOCOM 2002. Twenty-First Annual Joint Conference of the IEEE Computer and Communications Societies. Proceedings. IEEE*, vol. 3, pp. 1567–1576 vol.3, 2002.

[17] R. Vullers, R. Schaijk, H. Visser, J. Penders, and C. Hoof, "Energy harvesting for autonomous wireless sensor networks," *Solid-State Circuits Magazine, IEEE*, vol. 2, pp. 29–38, Spring 2010.

[18] S. Sudevalayam and P. Kulkarni, "Energy harvesting sensor nodes: Survey and implications," *Communications Surveys Tutorials, IEEE*, vol. 13, pp. 443–461, Third 2011.

[19] S. Ulukus, A. Yener, E. Erkip, O. Simeone, M. Zorzi, P. Grover, and K. Huang, "Energy harvesting wireless communications: A review of recent advances," *Selected Areas in Communications, IEEE Journal on*, vol. 33, pp. 360–381, March 2015.

[20] J. Yang and S. Ulukus, "Optimal packet scheduling in an energy harvesting communication system," *Communications, IEEE Transactions on*, vol. 60, pp. 220–230, January 2012.

[21] B. Devillers and D. Gunduz, "A general framework for the optimization of energy harvesting communication systems with battery imperfections," *J. Commun. Netw.*, vol. 14, pp. 130–139, April 2012.

[22] K. Tutuncuoglu, A. Yener, and S. Ulukus, "Optimum policies for an energy harvesting transmitter under energy storage losses," *Selected Areas in Communications, IEEE Journal on*, vol. 33, pp. 467–481, March 2015.

[23] N. Michelusi, K. Stamatiou, and M. Zorzi, "Transmission policies for energy harvesting sensors with time-correlated energy supply," *Communications, IEEE Transactions on*, vol. 61, pp. 2988–3001, July 2013.

[24] A. Biason and M. Zorzi, "Transmission policies for an energy harvesting device with a data queue," in *Computing, Networking and Communications (ICNC), 2015 International Conference on*, pp. 189–195, Feb 2015.

[25] H. Liu, A. Chandra, and J. Srivastava, "esense: Energy efficient stochastic sensing framework scheme for wireless sensor platforms," in *Proceedings of the 5th International Conference on Information Processing in Sensor Networks*, IPSN '06, (New York, NY, USA), pp. 235–242, ACM, 2006.

[26] J. Geng and L. Lai, "Non-Bayesian quickest change detection with stochastic sample right constraints," *Signal Processing, IEEE Transactions on*, vol. 61, pp. 5090–5102, Oct 2013.

[27] N. Edalat, M. Motani, J. Walrand, and L. Huang, "A methodology for designing the control of energy harvesting sensor nodes," *Selected Areas in Communications, IEEE Journal on*, vol. 33, pp. 598–607, March 2015.

[28] V. Joseph, V. Sharma, and U. Mukherji, “Optimal sleep-wake policies for an energy harvesting sensor node,” in *Communications, 2009. ICC ’09. IEEE International Conference on*, pp. 1–6, June 2009.

[29] A. Seyedi, “Controlled sampling using an energy harvesting sensor,” in *Information Theory and Applications Workshop (ITA), 2014*, pp. 1–5, Feb 2014.

[30] C. Schurgers, V. Tsiatsis, S. Ganeriwal, and M. Srivastava, “Optimizing sensor networks in the energy-latency-density design space,” *IEEE Transactions on Mobile Computing*, vol. 1, pp. 70–80, Jan 2002.

[31] M. Gorlatova, A. Wallwater, and G. Zussman, “Networking low-power energy harvesting devices: Measurements and algorithms,” in *INFOCOM, 2011 Proceedings IEEE*, pp. 1602–1610, April 2011.

[32] R. Chan, P. Zhang, W. Zhang, I. Nevat, A. Valera, H.-X. Tan, and N. Gautam, “Adaptive duty cycling in sensor networks via Continuous Time Markov Chain modelling,” in *Communications (ICC), 2015 IEEE International Conference on*, pp. 6669–6674, June 2015.

[33] J. Yang, X. Wu, and J. Wu, “Adaptive sensing scheduling for energy harvesting sensors with finite battery,” in *Communications (ICC), 2015 IEEE International Conference on*, pp. 98–103, June 2015.

[34] C. Vigorito, D. Ganesan, and A. Barto, “Adaptive control of duty cycling in energy-harvesting wireless sensor networks,” in *Sensor, Mesh and Ad Hoc Communications and Networks, 2007. SECON ’07. 4th Annual IEEE Communications Society Conference on*, pp. 21–30, June 2007.

[35] A. Kansal, J. Hsu, S. Zahedi, and M. B. Srivastava, “Power management in energy harvesting sensor networks,” *ACM Trans. Embed. Comput. Syst.*, vol. 6, Sep 2007.

[36] B. Medepally, N. Mehta, and C. Murthy, “Implications of energy profile and storage on energy harvesting sensor link performance,” in *Global Telecommunications Conference, 2009. GLOBECOM 2009. IEEE*, pp. 1–6, Nov 2009.

[37] C. K. Ho, P. D. Khoa, and P. C. Ming, "Markovian models for harvested energy in wireless communications," in *Communication Systems (ICCS), 2010 IEEE International Conference on*, pp. 311–315, Nov 2010.

[38] A. Ammar and D. Reynolds, "An adaptive scheduling scheme for cooperative energy harvesting networks," *Communications and Networks, Journal of*, vol. 17, pp. 256–264, June 2015.

[39] M.-L. Ku, Y. Chen, and K. Liu, "Data-driven stochastic models and policies for energy harvesting sensor communications," *Selected Areas in Communications, IEEE Journal on*, vol. 33, pp. 1505–1520, Aug 2015.

[40] A. Seyedi and B. Sikdar, "Energy efficient transmission strategies for body sensor networks with energy harvesting," *Communications, IEEE Transactions on*, vol. 58, pp. 2116–2126, July 2010.

[41] B. T. Bacinoglu and E. Uysal-Biyikoglu, "Finite-horizon online transmission rate and power adaptation on a communication link with Markovian energy harvesting," *CoRR*, vol. abs/1305.4558, 2013.

[42] V. Sharma, U. Mukherji, V. Joseph, and S. Gupta, "Optimal energy management policies for energy harvesting sensor nodes," *Wireless Communications, IEEE Transactions on*, vol. 9, pp. 1326–1336, April 2010.

[43] P. Poggi, G. Notton, M. Muselli, and A. Louche, "Stochastic study of hourly total solar radiation in Corsica using a Markov model," *International Journal of Climatology*, vol. 20, pp. 1843–1860, Nov 2000.

[44] S. Zhang, A. Seyedi, and B. Sikdar, "An analytical approach to the design of energy harvesting wireless sensor nodes," *Wireless Communications, IEEE Transactions on*, vol. 12, pp. 4010–4024, August 2013.

[45] N. Jaggi, K. Kar, and A. Krishnamurthy, "Near-optimal activation policies in rechargeable sensor networks under spatial correlations," *ACM Trans. Sen. Netw.*, vol. 4, pp. 17:1–17:36, Jun 2008.

[46] P. Lee, Z. A. Eu, M. Han, and H. Tan, "Empirical modeling of a solar-powered energy harvesting wireless sensor node for time-slotted operation,"

in *Wireless Communications and Networking Conference (WCNC), 2011 IEEE*, pp. 179–184, March 2011.

[47] J. Lei, R. Yates, and L. Greenstein, "A generic model for optimizing single-hop transmission policy of replenishable sensors," *Wireless Communications, IEEE Transactions on*, vol. 8, pp. 547–551, Feb 2009.

[48] H. Kantz, D. Holstein, M. Ragwitz, and N. K. Vitanov, "Markov chain model for turbulent wind speed data," *Physica A: Statistical Mechanics and its Applications*, vol. 342, no. 12, pp. 315 – 321, 2004. Proceedings of the VIII Latin American Workshop on Nonlinear Phenomena.

[49] S. Asmussen and H. Albrecher, *Ruin Probabilities.* World Scientific, second ed., 2010.

[50] S. Asmussen, F. Avram, and M. Usabel, "Erlangian approximations for finite-horizon ruin probabilities," *Astin Bulletin*, vol. 32, no. 2, pp. 267–282, 2002.

[51] M. A. Yazici and N. Akar, "The finite/infinite horizon ruin problem with multi-threshold premiums: a Markov fluid queue approach." To appear at Annals of Operations Research, 2016.

[52] G. Jones, P. Harrison, U. Harder, and T. Field, "Fluid queue models of battery life," in *Modeling, Analysis Simulation of Computer and Telecommunication Systems (MASCOTS), 2011 IEEE 19th International Symposium on*, pp. 278–285, July 2011.

[53] N. Gautam and A. Mohapatra, "Efficiently operating wireless nodes powered by renewable energy sources," *Selected Areas in Communications, IEEE Journal on*, vol. 33, pp. 1706–1716, Aug 2015.

[54] V. G. Kulkarni in *Frontiers in Queueing: Models and Applications in Science and Engineering* (J. H. Dshalalow, ed.), ch. Fluid Models for Single Buffer Systems, pp. 321–338, Boca Raton, FL, USA: CRC Press, Inc., 1997.

[55] M. Mandjes, D. Mitra, and W. Scheinhardt, "Models of network access using feedback fluid queues," *Queueing Syst. Theory Appl.*, vol. 44, pp. 365–398, Aug 2003.

[56] N. Akar and K. Sohraby, "Infinite- and finite-buffer Markov fluid queues: a unified analysis," *J. Appl. Probab.*, vol. 41, pp. 557–569, 06 2004.

[57] H. E. Kankaya and N. Akar, "Solving multi-regime feedback fluid queues," *Stochastic Models*, vol. 24, no. 3, pp. 425–450, 2008.

[58] M. A. Yazici and N. Akar, "Analysis of continuous feedback Markov fluid queues and its applications to modeling optical burst switching," in *Teletraffic Congress (ITC), 2013 25th International*, pp. 1–8, Sept 2013.

[59] M. A. Yazici, *Stochastic Modeling with Continuous Feedback Markov Fluid Queues*. PhD thesis, Bilkent University, Jan 2014.

[60] G. H. Golub and C. F. Van Loan, *Matrix Computations (3rd Ed.)*. Baltimore, MD, USA: Johns Hopkins University Press, 1996.

[61] H. E. Kankaya, *Performance Evaluation of Telecommunication Networks Based on Multi-Regime Fluid Queues*. PhD thesis, Bilkent University, July 2009.

[62] W. Heinzelman, A. Chandrakasan, and H. Balakrishnan, "Energy-efficient communication protocol for wireless microsensor networks," in *System Sciences, 2000. Proceedings of the 33rd Annual Hawaii International Conference on*, pp. 10 pp. vol.2–, Jan 2000.

[63] U. of Oregon Solar Radiation Laboratory, "Northwest solar resource maps," Jul 2013.

Appendix A

Appendix

A.1 Numerical Example

We consider a two-state EHP with $\lambda_{min} = 1$, $\lambda_{max} = 2$, $u = B = 3000$, $B_0 = B_1 = 1500$, $\boldsymbol{\alpha} = \begin{bmatrix} 5/6 & 1/6 \end{bmatrix}$, $l = 1$, $H = 1$ months (720 hours), $\eta = l/H \approx 0.0014$, $l_b = 1.25$, $p_T = 10$, $\beta = 0.45$, $p_0 = 0$, $p_1 = 120$ and

$$Q = \begin{bmatrix} -1/5 & 1/5 \\ 1 & -1 \end{bmatrix}$$

which is the infinitesimal generator matrix of the EHP. Since the thresholds B_0 and B_1 are equal, this set of parameters gives rise to a two-regime MFQ with regime boundaries $T^{(0)} = 0$, $T^{(1)} = 1500$ and $T^{(2)} = 3000$. From the expressions in (3.3), (3.4) and (3.5), one can write the infinitesimal generators $Q^{(1)}$, $Q^{(2)}$, $\tilde{Q}^{(0)}$, $\tilde{Q}^{(1)}$ and $\tilde{Q}^{(J)} = \tilde{Q}^{(2)}$ as follows:

$$
Q^{(1)} = \tilde{Q}^{(1)} = \begin{bmatrix} 0 & 0 & 0 & 0 & 0 & 0 & 0 \\ 0 & 0 & 0 & 0 & 0 & 0 & 0 \\ 0 & 0 & 0 & 0 & 0 & 0 & 0 \\ 0 & 0 & 0.0014 & -1.2014 & 0.2 & 1 & 0 \\ 0 & 0 & 0.0014 & 1 & -2.0014 & 0 & 1 \\ 0 & 0 & 0 & 0.45 & 0 & -0.45 & 0 \\ 0 & 0 & 0 & 0 & 0.45 & 0 & -0.45 \end{bmatrix},
$$

$$
Q^{(2)} = \begin{bmatrix} 0 & 0 & 0 & 0 & 0 & 0 & 0 \\ 0 & 0 & 0 & 0 & 0 & 0 & 0 \\ 0 & 0 & 0 & 0 & 0 & 0 & 0 \\ 0 & 0 & 0.0014 & -2.2014 & 0.2 & 2 & 0 \\ 0 & 0 & 0.0014 & 1 & -3.0014 & 0 & 2 \\ 0 & 0 & 0 & 0.45 & 0 & -0.45 & 0 \\ 0 & 0 & 0 & 0 & 0.45 & 0 & -0.45 \end{bmatrix},
$$

$$
\tilde{Q}^{(0)} = \begin{bmatrix} 0 & 0 & 0 & 0 & 0 & 0 & 0 \\ 0 & 0 & 0 & 0 & 0 & 0 & 0 \\ 0 & 1 & -1 & 0 & 0 & 0 & 0 \\ 1 & 0 & 0 & -1 & 0 & 0 & 0 \\ 1 & 0 & 0 & 0 & -1 & 0 & 0 \\ 1 & 0 & 0 & 0 & 0 & -1 & 0 \\ 1 & 0 & 0 & 0 & 0 & 0 & -1 \end{bmatrix},
$$

$$
\tilde{Q}^{(J)} = \tilde{Q}^{(2)} = \begin{bmatrix} -1 & 0 & 0 & 0.8333 & 0.1667 & 0 & 0 \\ 0 & -1 & 0 & 0.8333 & 0.1667 & 0 & 0 \\ 0 & 0 & 0 & 0 & 0 & 0 & 0 \\ 0 & 0 & 0.0014 & -2.2014 & 0.2 & 2 & 0 \\ 0 & 0 & 0.0014 & 1 & -3.0014 & 0 & 2 \\ 0 & 0 & 0 & 0.45 & 0 & -0.45 & 0 \\ 0 & 0 & 0 & 0 & 0.45 & 0 & -0.45 \end{bmatrix}.
$$

Similarly, regime and boundary drift matrices can be written from (3.6) and (3.7) as follows:

$$R^{(1)} = R^{(2)} = \tilde{R}^{(1)} = \begin{bmatrix} 1 & 0 & 0 & 0 & 0 & 0 & 0 \\ 0 & 1 & 0 & 0 & 0 & 0 & 0 \\ 0 & 0 & -1 & 0 & 0 & 0 & 0 \\ 0 & 0 & 0 & -1.25 & 0 & 0 & 0 \\ 0 & 0 & 0 & 0 & 118.75 & 0 & 0 \\ 0 & 0 & 0 & 0 & 0 & -10 & 0 \\ 0 & 0 & 0 & 0 & 0 & 0 & -10 \end{bmatrix},$$

$$\tilde{R}^{(0)} = \begin{bmatrix} 1 & 0 & 0 & 0 & 0 & 0 & 0 \\ 0 & 1 & 0 & 0 & 0 & 0 & 0 \\ 0 & 0 & 0 & 0 & 0 & 0 & 0 \\ 0 & 0 & 0 & 0 & 0 & 0 & 0 \\ 0 & 0 & 0 & 0 & 118.75 & 0 & 0 \\ 0 & 0 & 0 & 0 & 0 & 0 & 0 \\ 0 & 0 & 0 & 0 & 0 & 0 & 0 \end{bmatrix},$$

$$\tilde{R}^{(2)} = \begin{bmatrix} 0 & 0 & 0 & 0 & 0 & 0 & 0 \\ 0 & 0 & 0 & 0 & 0 & 0 & 0 \\ 0 & 0 & -1 & 0 & 0 & 0 & 0 \\ 0 & 0 & 0 & -1.25 & 0 & 0 & 0 \\ 0 & 0 & 0 & 0 & 0 & 0 & 0 \\ 0 & 0 & 0 & 0 & 0 & -10 & 0 \\ 0 & 0 & 0 & 0 & 0 & 0 & -10 \end{bmatrix}.$$

Then, by following the procedure described in Section 2.3, one can obtain $A_-^{(k)}$, $A_+^{(k)}$, $L_0^{(k)}$, $L_-^{(k)}$ and $L_+^{(k)}$ for $k = 1, 2$ as follows:

$$A_-^{(1)} = -0.0018,\ A_+^{(1)} = \begin{bmatrix} 0.9976 & -0.3190 & -0.0067 \\ 0 & 0.0003 & -0.0003 \\ 0 & 0 & 0.0381 \end{bmatrix},$$

$$A_-^{(2)} = -0.0074,\ A_+^{(2)} = \begin{bmatrix} 1.8014 & -0.1913 & -0.0176 \\ 0 & 0.0001 & 0.0005 \\ 0 & 0 & 0.0318 \end{bmatrix},$$

$$L_0^{(1)} = \begin{bmatrix} 1 & 0 & 0 & 0 & 0 & 0 & 0 & 0 \\ 0 & 1 & 0 & 0 & 0 & 0 & 0 & 0 \\ 0 & 0 & 1 & 0 & 0 & 0 & 0 & 0 \end{bmatrix},$$
$$L_-^{(1)} = \begin{bmatrix} 0 & 0 & -19.8380 & -20.6974 & -5.0108 & -44.2253 & -10.7068 \end{bmatrix},$$
$$L_+^{(1)} = \begin{bmatrix} 0 & 0 & -0.6375 & -0.9162 & 0.0233 & 0.3956 & 0.0599 \\ 0 & 0 & -1.9974 & 0.4005 & 0.0770 & 0.8979 & 0.1656 \\ 0 & 0 & -0.0020 & -0.0124 & 0.0672 & -0.1812 & 0.9811 \end{bmatrix},$$

$$L_0^{(2)} = \begin{bmatrix} 1 & 0 & 0 & 0 & 0 & 0 & 0 & 0 \\ 0 & 1 & 0 & 0 & 0 & 0 & 0 & 0 \\ 0 & 0 & 1 & 0 & 0 & 0 & 0 & 0 \end{bmatrix},$$
$$L_-^{(2)} = \begin{bmatrix} 0 & 0 & -1.1706 & -4.1730 & -2.0563 & -15.9304 & -7.8500 \end{bmatrix},$$
$$L_+^{(2)} = \begin{bmatrix} 0 & 0 & -0.7066 & -0.9765 & 0.0044 & 0.2130 & 0.0316 \\ 0 & 0 & -6.6622 & 0.2149 & 0.0437 & 0.9539 & 0.2049 \\ 0 & 0 & -0.0022 & -0.0138 & 0.0644 & -0.2094 & 0.9756 \end{bmatrix},$$

which are required to solve for the unknowns in Eqn. (2.27).

At this point, we have all the matrices required to write the boundary conditions (2.8)-(2.17) in the matrix form $zH = b$ which is to be solved for the vector of unknowns z where matrix H is obtained by using the boundary conditions. If we solve for vector z for this particular example, we find the probability mass accumulations at boundary points $T^{(0)} = 0$, $T^{(1)} = 1500$ and $T^{(2)} = 3000$ as

$$c^{(0)} = 10^{-3}\begin{bmatrix}0 & 0 & 0.0939 & 0.0050 & 0 & 0.1052 & 0.0039\end{bmatrix},$$
$$c^{(1)} = \begin{bmatrix}0 & 0 & 0 & 0 & 0 & 0 & 0\end{bmatrix},$$
$$c^{(2)} = 10^{-3}\begin{bmatrix}0.1141 & 0.0939 & 0 & 0 & 0.1200 & 0 & 0\end{bmatrix}.$$

From Eqn. (3.8), we calculate the finite horizon battery outage probability as $\psi(u, \boldsymbol{\alpha}, H) = c_O^{(2)}/(c_O^{(2)} + c_R^{(2)}) = 0.1141/(0.1141 + 0.0939) = 0.5486$. Similarly, we obtain the unknowns in Eqn. (2.27) $a^{(k)} = [a_0^{(k)} \quad a_-^{(k)} \quad a_+^{(k)}]$ for $k = 1, 2$ as

$$a^{(1)} = 10^{-3}\begin{bmatrix}0.1141 & 0.0939 & 0.2080 & 0.0008 & 0.0162 & 0.0911 & 0.0176\end{bmatrix},$$
$$a^{(2)} = 10^{-3}\begin{bmatrix}0.1141 & 0.0939 & 0.2080 & -0.0035 & -0.2284 & 0.0554 & 0.0203\end{bmatrix},$$

from which steady-state joint pdf vector $f^{(k)}(x)$, $k = 1, 2$ is obtained from Eqn. (2.27). By using expression (3.10), we then calculate the following probabilities in each regime for each state:

$$\Pr\{Z(t) = 0, X(t) \le B_0\} = 0.7057,$$
$$\Pr\{Z(t) = 0, X(t) > B_0\} = 0.1275,$$
$$\Pr\{Z(t) = 1, X(t) \le B_1\} = 0.1309,$$
$$\Pr\{Z(t) = 1, X(t) > B_1\} = 0.0359.$$

Finally, multiplying these probabilities with the corresponding sensing rate values (as in Eqn. (3.11)) gives the average sensing rate as follows:

$$\begin{aligned}\lambda_{avg} = &\Pr\{Z(t) = 0, X(t) \le B_0\}\lambda_{min} + \Pr\{Z(t) = 0, X(t) > B_0\}\lambda_{max} \\ &+ \Pr\{Z(t) = 1, X(t) \le B_1\}\lambda_{min} + \Pr\{Z(t) = 1, X(t) > B_1\}\lambda_{max} \\ &= (0.7057 + 0.1309)\lambda_{min} + (0.1275 + 0.0359)\lambda_{max} \\ &= 1.1634.\end{aligned}$$